Measuring Two-Dimensional Receptor-Ligand Binding Kinetics by Micropipette

Scott E. Chesla,* Periasamy Selvaraj,# and Cheng Zhu*
*George W. Woodruff School of Mechanical Engineering, Georgia Institute of Technology, Atlanta, Georgia 30332-0405, and
#Department of Pathology and Laboratory Medicine, Emory University School of Medicine, Atlanta, Georgia 30322 USA

ABSTRACT We report a novel method for measuring forward and reverse kinetic rate constants, k_f^0 and k_r^0, for the binding of individual receptors and ligands anchored to apposing surfaces in cell adhesion. Not only does the method examine adhesion between a single pair of cells; it also probes predominantly a single receptor-ligand bond. The idea is to quantify the dependence of adhesion probability on contact duration and densities of the receptors and ligands. The experiment was an extension of existing micropipette protocols. The analysis was based on analytical solutions to the probabilistic formulation of kinetics for small systems. This method was applied to examine the interaction between Fcγ receptor IIIA (CD16A) expressed on Chinese hamster ovary cell transfectants and immunogobulin G (IgG) of either human or rabbit origin coated on human erythrocytes, which were found to follow a monovalent biomolecular binding mechanism. The measured rate constants are $A_c k_f^0 = (2.6 \pm 0.32) \times 10^{-7}$ μm^4 s^{-1} and $k_r^0 = (0.37 \pm 0.055)$ s^{-1} for the CD16A-hIgG interaction and $A_c k_f^0 = (5.7 \pm 0.31) \times 10^{-7}$ μm^4 s^{-1} and $k_r^0 = (0.20 \pm 0.042)$ s^{-1} for the CD16A-rIgG interaction, respectively, where A_c is the contact area, estimated to be a few percent of 3 μm^2.

INTRODUCTION

Controlling when, how, and to what cells adhere is important in both biological and clinical settings. Adhesion governs the integrity of biological tissues as well as communication between cells and their environment. Adhesion is also the critical biological process determining the effectiveness of cell separation devices used in stem cell isolation and chemotherapy procedures (Berenson et al., 1986). In the immune system, binding of antibody-antigen complexes to leukocyte Fc receptors initiates important effector functions (Unanue, 1984).

Cell adhesion is mediated by specific (so-called lock-and-key) interactions between receptors and ligands. Such interactions can be better modeled by reaction kinetics than a force-distance relationship, although the latter is commonly used to describe nonspecific interactions (Bell, 1978; Leckband et al., 1994). As such, the kinetic rate constants of surface-bound receptor-ligand binding are an essential determinant of cell adhesion, for these parameters describe how rapidly cells bind and how long they remain bound. The physiological relevance of kinetic rates can be clearly exemplified by the multiple adhesion pathways involved in the recruitment of leukocytes from the circulation to the inflamed tissue. The adhesive interactions of leukocytes with the vascular endothelium consist of two consecutive steps: rolling and firm adhesion, which are mediated, respectively, by two distinct classes of adhesion molecules: selectins and integrins (Lawrence and Springer, 1991; von Andrian et al., 1991). The ability of the selectins to mediate rolling is believed to be due, at least in part, to a peculiar property of these molecules: their rapid kinetic rates, which enable the selectins to effectively capture their carbohydrate ligands when leukocytes are traveling in the bloodstream with a velocity as high as 100 cell diameters per second and hence are colliding with the stationary vascular wall for a contact duration as short as milliseconds (Pierres et al., 1996a). Rolling slows the leukocytes down, and thereby increases their contact duration with the endothelium and enables them to sense signals that activate the integrins, which allows the integrins with slower kinetic rates to engage in firm adhesion.

Despite the obvious importance of kinetic rate constants to our understanding of various cell adhesion processes, not until very recently have they been directly determinable experimentally. To date, only a handful of such measurements exist in the literature (Kaplanski et al., 1993; Pierres et al., 1995; Alon et al., 1995, 1997; Chen et al., 1997; Tees et al., 1993; Tees and Goldsmith, 1996; Kwong et al., 1996). The reason for this gap in knowledge lies in the lack of experimental methodology. Although there are many methods of measuring receptor-ligand binding kinetics when at least one of the molecular species is in solution (i.e., three-dimensional kinetics), none of these methods can be applied when the two molecules are bound to two apposed surfaces, as in the case of cell-cell or cell-substrate adhesion (i.e., two-dimensional kinetics) (Piper et al., 1998).

This inapplicability of the existing methods is due to the fact that they all require quantification of the concentration changes of the bound and free ligands with time. However, in cell adhesion assays one usually measures only the fraction of adherent or detached cells. Although there is no adhesive bond associated with a detached cell, the number of bonds on an adherent cell can vary from one up. The only published method for measuring the bond density using

Received for publication 8 January 1998 and in final form 14 May 1998.
Address reprint requests to Dr. Cheng Zhu, School of Mechanical Engineering, Georgia Institute of Technology, Atlanta, GA 30322-0363. Tel.: 404-894-3269; Fax: 404-894-2291; E-mail: cheng.zhu@me.gatech.edu.

0006-3495/98/09/1553/20 $2.00

fluorescent labeling requires a 30-min incubation to allow lateral diffusion of the unbound molecules inside and outside of the contact area to reach the steady state (Dustin et al., 1996), which is far longer than the kinetic transient time of many receptor-ligand interactions, including the ones studied in the present work. Therefore, only 2D binding affinity, not kinetic rates, can be measured by the method of Dustin et al. (1996). To the best of our knowledge, no method exists that allows direct measurement of the changes in the density of bonds with time when the receptor-ligand bonds are localized inside the contact area spanning a narrow gap between two cells or between a cell and a substrate surface.

Because of the inability to directly measure the time course of bond density, the kinetics of receptor-ligand binding has to be inferred from the changes in the fraction of adherent cells with time and its relation to the distribution of bonds among these cells. Kaplanski et al. (1993) were the first to employ this idea to measure adhesion kinetics. To date, all of the published work on adhesion kinetics measurements used flow techniques (Kaplanski et al., 1993; Pierres et al., 1995; Alon et al., 1995, 1997; Chen et al., 1997; Tees et al., 1993; Tees and Goldsmith, 1996; Kwong et al., 1996). In the flow chamber, the kinetic rates were estimated by analyzing the probabilities of forming a durable adhesion per unit length of travel between a cell and the surface and of the duration of these adhesions. A problem inherent to the flow chamber method is the lack of ability to control the adhesion event. It is difficult to determine (let alone control) from a top view observation whether a moving cell is in transient contact (i.e., colliding) with the surface until it is arrested (Pierres et al., 1996a, b). Therefore, the measured adhesion probability per unit displacement is a lumped parameter. It depends not only on the fraction of contacts that yield adhesion (adhesion probability per contact), but also on the number of contacts per unit length of travel (collision frequency), as well as on the duration and area of each contact. None of these can be measured separately and independently in the flow chamber system. Moreover, the formation of the first bond (which requires capture of the rapidly moving cell from the flow) is very different from that of the subsequent bonds (which involves receptor-ligand binding between two surfaces with much less relative motion) (Kaplanski et al., 1993). In addition, the size of the contact area, the duration of the contact, and the force exerted on the contact cannot be controlled by the experimenter, and they are all variable rather than constant in the flow chamber system. These difficulties make the estimate of the forward rate constant ambiguous. Determination of the reverse rate constant, in contrast, is much simpler, because it involves only measurements of the lifetime of durable adhesions (Alon et al., 1995, 1997; Chen et al., 1997).

We have developed a novel method for measuring adhesion kinetics that uses the micropipette technique. The basic idea is to directly measure the adhesion probability per contact, rather than per unit length of travel, by controlling both the collision frequency and the contact duration. Our micropipette procedure is an extension of that of Evans (Evans et al., 1991, 1995), which uses an ultrasensitive red blood cell (RBC) picoforce transducer to detect adhesion mediated by a low number of receptor-ligand bonds (Fig. 1). Our modifications include repeating the adhesion tests hundreds of times with the same pair of cells, controlling the duration and area of the contact in these tests, and counting the fraction of adhesive events resulting from all of the tests. In contrast to the classical micropipette adhesion assays (Sung et al., 1986), which involve a large number of bonds and definitive binding in every test, our experiment is designed to work in a regime in which adhesion occurs randomly in only some of the tests. We are not concerned with the adhesion strength but rather with the adhesion probability, which is determined from the running frequency of the binding events. The adhesion probability varies between zero and one, and its dependence on contact duration provides the information regarding kinetic rates.

The advantage of the micropipette procedure is obvious. The experimenter not only observes, but also controls the adhesion event: when the contact begins and ends, how hard the two cells are pressed against each other to form how small a contact area, and what ramp force is applied to separate the contact. With the micropipette, each "collision" between the two cells is controlled via precise micromanipulation, as opposed to the flow chamber experiment in which the contact of a moving cell with the stationary surface is fairly random. Each contact is controlled for a predetermined duration regardless of whether actual adhesion occurs, as opposed to the flow chamber experiment, in which one can detect only those contacts that result in durable adhesion without any control or knowledge of the time elapsed from the contact beginning to the formation of the first bond. Thus all of the aforementioned difficulties in flow chamber are eliminated. The cost of increased experimental control over the adhesion events is in terms of time, as only one interaction between a single pair of cells may be tested at a time in the micropipette experiment.

To extract the kinetic information from the measured adhesion probability versus contact time data requires a model of the underlying receptor-ligand interaction. We have adapted McQuarrie's (1963; Cozens-Roberts et al., 1990) probabilistic formulation of kinetics in small systems and solved the master equations analytically. These closed-form solutions greatly facilitate analysis of the data. In addition, they allowed for systematic examination of the order of the reactions to identify the kinetic mechanism most appropriate for the data.

The method was validated experimentally by using a biological system that consisted of CD16A expressed in Chinese hamster ovary (CHO) cell transfectants binding to IgG of either human or rabbit origin coated on human RBC. CD16A is a Fc gamma receptor (FcγRIIIA) that is vital to the immune system. It is a 50–80-kDa cell surface glycoprotein expressed on macrophages, natural killer cells, and subsets of monocytes and T lymphocytes. Upon binding to

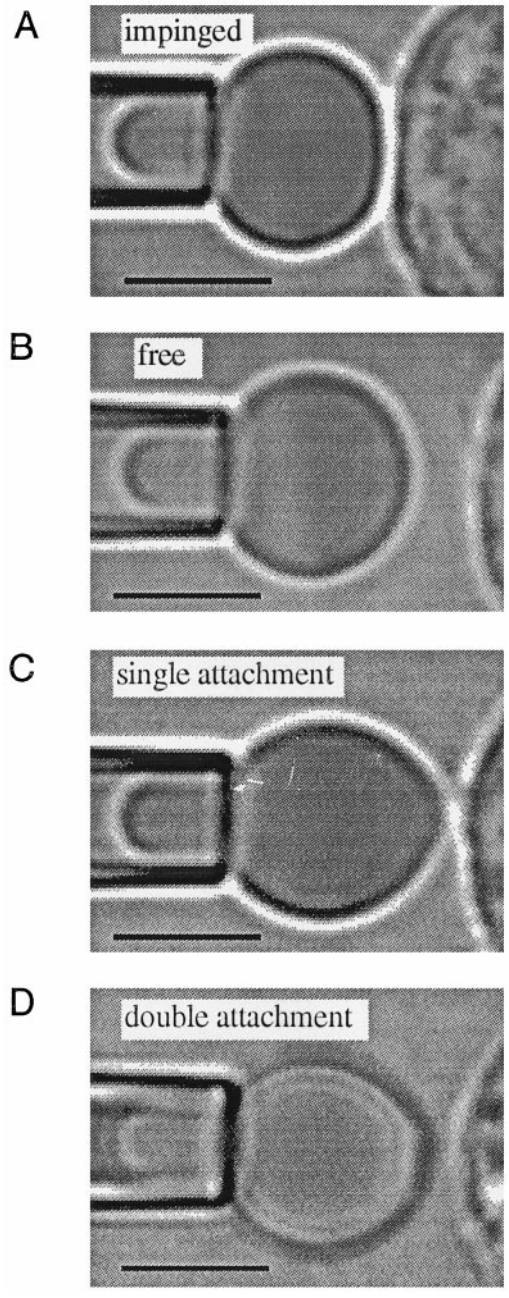

FIGURE 1 Photomicrographs of a typical adhesion test involving an IgG-coated RBC aspirated by a micropipette (*left*) and a CD16A-expressing CHO cell, aspirated by another micropipette (only partially shown, *right*). (*A*) The RBC was brought into contact with the CHO cell with an overall apparent contact diameter of ~2 μm. The contact area and time between the CHO and RBC cells were carefully controlled. (*B*) The unaspirated portion of the RBC is shown in its free, spherical shape. (*C*) A retracting RBC that was previously allowed to adhere to a CHO cell. The attachment site between the two cells appears as a single point in the microscopic image. (*D*) The retracting RBC adheres to the CBO cell to the CHO cell via two spatially distinctly separate point attachments. Note that the RBC elongations in *C* and *D* from the undeformed shape in *B* allow adhesions to be easily and unambiguously detected. The bar represents 5 μm.

the Fc portion of IgG, a wide variety of effector responses can be triggered by CD16, including clearance of immune complex, receptor-mediated phagocytosis, antibody-dependent cellular cytotoxicity, release of inflammatory mediators, and enhancement of antigen presentation, to name a few (Hulett and Hogarth, 1994; van de Winkel and Capel, 1993). The CD16-IgG binding is known to be of low affinity, and as such cannot be directly measured via Scatchard analysis (Chesla et al., 1995). Here we report for the first time measurements of the 2D kinetic rate constants for this receptor-ligand interaction. In addition, we compare the kinetic rates of CD16A binding to IgG ligands from two different origins, human and rabbit.

MATERIALS AND METHODS

Cells and antibodies

Our CHO cells transfected to express human CD16A have previously been described (Nagarjan et al., 1995). The control CHO cells (untransfected, K1 and transfected to express $\alpha_{IIb}\beta_3$, A5) were generous gifts from Dr. Mark H. Ginsberg (Scripps Research Institute, La Jolla, CA). CHO cells were cultured in Roswell Park Memorial Institute (RPMI) 1640 media (Sigma, St. Louis, MO) supplemented with 2 mM L-glutamine (Sigma), and 10% fetal bovine serum (FBS) (Gibco BRL, Grand Island, NY). For the CD16A transfectants, 400 μg/ml geneticin (Life Technologies, Gaithersburg, MD) was included in the culture media as a selection antibiotic to suppress the nontransfected cells. The expression of CD16A was periodically checked via flow cytometry. Because the micropipette is a single-cell assay and cell-to-cell variations contribute significantly to experimental deviation, a homogeneous cell population expressing a uniform level of CD16A is desirable. To obtain homogeneous populations of cells expressing different receptor densities, CHO cells were sorted through a FACSort (Becton Dickinson, San Jose, CA). The tight receptor expression distributions in the sorted populations lasted ~1 month before the cells returned to their original, more heterogeneous characteristics.

Observing approved NIH guidelines, fresh blood from healthy donors was collected by venipuncture into sterile vacutainers (Becton Dickinson) with EDTA as an anticoagulant. Tubes were refrigerated for 4 h to allow serum separation. The RBC fraction was collected, washed twice in RPMI 1640 with 5% FBS, and then stored at 5°C. These cells could be used for up to ~2 weeks, after which lysis of the RBCs became apparent.

Total human IgG (hIgG) (Lampire, Pipersville, PA) and rabbit IgG (rIgG) (Sigma) were used as ligands for CD16A. The fluorescein isothiocyanate (FITC)-coupled goat polyclonal anti-human, anti-rabbit, and anti-mouse antibodies used in flow cytometry were purchased from Sigma. The monoclonal antibody (mAb) Leu-11b (mouse IgM) specifically directed against CD16 was purchased from Becton Dickinson. Another anti-CD16 mAb Fcgran1 CLB (mouse IgG2a) and the irrelevant control mAb X63 (mouse IgG1) were produced in house as previously described (Nagarjan et al., 1995). The fragmentation of CLB into Fc and Fab subunits was done by Lampire. The genetically engineered dimeric soluble form of CD16A (sCD16A) and the control soluble molecule B7 (sB7) were produced by our laboratory and will be described in detail elsewhere (Li et al., manuscript in preparation).

Coating of ligands

Ligand was coated onto RBCs by a standard chromium chloride ($CrCl_3$) coupling protocol (Gold and Fudenberg, 1967; Kofler and Wilk, 1977). Briefly, 10^8 RBCs were suspended in 250 μl saline (4% hematocrit). When ligand (hIgG, rIgG, or a control protein bovine serum albumen (BSA); Sigma) in phosphate-free medium (typically at 10 μg/ml) was added along with 250 μl of 0.001% $CrCl_3$ solution in 0.02 M acetate buffer, pH 5.5, spontaneous coupling occurred. After 5 min the reaction was quenched with phosphate-buffered saline (PBS), 5 mM EDTA with 1% BSA. RBCs were used immediately after protein coating. This coupling reaction is accomplished almost immediately and is thought to involve the chemical

bonding of protein carboxyl groups with membrane proteins on the RBC. The reaction is nonspecific, the orientation of the coated protein with respect to the membrane is most likely random, and the ligand density has to be determined for each reaction to circumvent variability in the coating. Nevertheless, the method is extremely efficient in terms of time, coating densities, and minimum alteration of RBC membrane characteristics.

Determination of receptor and ligand densities

The surface densities of receptors and ligands were determined primarily via flow cytometry analysis. Samples of RBCs used in the micropipette experiment were incubated with FITC-labeled goat anti-human or anti-rabbit antibodies, depending on the origin of the coated IgG ligands. For negative controls, the hIgG (or rIgG)-coated RBCs were incubated with the FITC-labeled goat anti-rabbit (or anti-human) antibodies. CHO cell samples were first preincubated with the mouse anti-CD16 mAb Fcgran1 CLB (or without a primary antibody for control) and then with a FITC-labeled goat anti-mouse polyclonal secondary antibody. The fluorescent intensities of the cells were compared to standard calibration beads (Flow Cytometry Standards Corp., San Juan, PR) to determine the mean number of events per particle, which was directly converted into labeled protein per cell with manufacturer-provided software.

Receptor densities on different CHO cell populations were cross-checked by radioimmunoassay. Fab fragments of CLB were iodinated using Iodo-Gen (Pierce, Rockford, IL) (Selvaraj et al., 1988). CHO cells were incubated in titrated concentrations of CLB-Fab, and the bound fraction was determined with a gamma counter. Scatchard analysis (Scatchard, 1949) was employed to derive the (3D) affinity (of CD16A-CLB binding) and the (average) receptor number per cell, which was then divided by the apparent area of the spherical cell to convert to surface density.

The micropipette system

The micropipette system used in this laboratory was designed, built, and calibrated in house; the majority of the components were purchased off the shelf (Delobel, 1992). It is similar to those established in other laboratories (Paul Sung, University of California at San Diego; Evan Evans, University of British Columbia; Robert Hochmuth, Duke University). The system consists of video-enhanced optical microscopy, micromanipulation, and pressure regulation subsystems.

The centerpiece of the microscopic system is a Zeiss inverted microscope (Axiovert 100; Oberkochan, Germany) with a 100× oil immersion, 1.25 N.A. objective. Diffraction is minimized with a green light (546-nm wavelength) band-pass (5-nm bandwidth) filter that also reduces any photochemical damage to the RBC. Additional magnification is obtained using a 5× relay lens, leading to a charge-coupled device (CCD) camera (model 72S; Dage-MTI, Michigan City, IN). A digital image processor (model DSP-2000; Dage-MTI) is used to enhance the image. The signal also passes through a digital voltage multiplexer (model 401; Vista Electronics, Ramona, CA), which allows video integration and display of a timer on screen. Recording is accomplished using a super VHS video cassette recorder (model AG-7355; Panasonic, Secaucus, NJ). A video monitor (Panasonic) displays the image at a final magnification of ~2500× as calibrated by a stage micrometer.

Micropipettes are made from borosilicate glass tubing (Richland Glass, Richland, NJ) with an outside diameter of 1 mm and an inside diameter of 0.7 mm. To guarantee clean pipettes, the original glass tubing is cleaned with acetone, cleaned a second time in a boiling solution of 50% ethanol for 1 h, and dried again. A two-step process is used with the first, utilizing a micropipette puller (model 700D; Kopf, Tujunga, CA). Next, a microforge (built in house, similar to commercial models, except that a glass bead is added to the filament, adapted from the laboratory of Robert M. Hochmuth, Duke University, Durham, NC) is used to break the micropipette with a flush tip at the desired diameter. The pipettes are connected to the pressure regulation system through stainless steel injection holders. Each pipette can be coarsely manipulated by a mechanical drive mounted on the microscope and finely positioned with a three-axis hydraulic micromanipulator (Narishige, Tokyo, Japan). In addition, one of the pipette holders is mounted on a piezo translator (Physik Instrumente, Waldbronne, Germany), the driver of which is controlled by a computer to achieve precise and repeatable movement of the pipette in an adhesion test cycle. To avoid vibration of the micropipettes during the experiment, the microscope, along with the micromanipulators, is seated on an air suspension table (Kinetics Systems, Boston, MA).

The pressure regulation subsystem is used to control suction during the experiment and is critical for tuning the sensitivity of the RBC picoforce transducer. A hydraulic line connects the micropipette holder to a fluid reservoir. The centerpiece of the design is a fine jack that allows the height of the reservoir to be precisely manipulated. A metric long-range dial indicator (Starrett, Athol, MA) was attached to the reservoir to measure its position and therefore the applied vacuum pressure in mm H_2O.

Micropipette adhesion test cycle

CHO cells were removed from flasks with 5 mM EDTA/PBS, washed twice in RPMI, and then stored on ice until injection into the micropipette chamber. The chamber consists of two coverslips attached to a stainless steel holder on the top and bottom to allow optical imaging, while open on two sides to allow micropipette access. The solution used in the chamber during the experiment was half isotonic (1:1 distilled H_2O and Hanks' balanced salt solution (HBSS) without Ca^{+2} (Sigma) and 1% BSA), which caused the RBCs to swell to nearly spherical shape, but had no detectable effect on the CHO cells' viability, consistent with the report of a recent paper (Setiadi et al., 1998) that CHO cells have a high tolerance to variations in the ionic strength in the culture medium. After single CHO and RBC cells were captured and positioned with the apposing pipettes, the computer program for repeated adhesion test cycles was initiated, with the movement of the RBCs precisely driven by the piezo translator and the CHO cell held stationary (Fig. 1).

An adhesion test cycle consists of impinging the RBC into controlled contact (Fig. 1 *A*), allowing the contact to continue for a predetermined incubation time, then retracting the RBC from the CHO cell at a predetermined rate and observing any adhesions. The contact area is managed by controlling the amount of RBC impingement on the CHO cell surface. Because the piezo-controlled RBC returns to the same location after every adhesion stroke attempt, impingement is controlled by manual adjustment of the CHO cell location. In this way, the contact area and location were held essentially constant.

Adhesions could easily be unambiguously distinguished from nonadhesions (Fig. 1 *B*) by deflections in the RBC surface at the area of contact (Fig. 1, *C* and *D*). Most observed adhesions were point attachments near the apex of the RBC (Fig. 1 *C*). Multiple point attachments were also occasionally detected (Fig. 1 *D*), especially at higher adhesion frequencies. The outcome of each test was scored as one if adhesion resulted, and as zero if not.

The adhesion test cycle was then repeated at the same contact area. Typically a sequence of 50–200 such repeated tests was performed with the same pair of cells. The binary adhesion scores were averaged up to the most recent test, and this running frequency of adhesion was plotted against the test cycle count for a given sequential test series. It is the analysis of this running frequency that yields an estimate of the adhesion probability per contact.

Data analysis

The theoretical solutions were fitted to the experimental data by a numerical routine that employs the Levenberg-Marquart method to evaluate the parameters that minimize the sum of squared weighted (by the reciprocal standard deviations) errors (χ^2) between the data and the predictions (Press et al., 1989). The program also uses the spread and standard deviation of the data to estimate the standard deviations of the fitted parameters. To

determine the most appropriate kinetic mechanism, the goodness of fit of various models as measured by the χ^2 values for the same data set were compared (Piper et al., 1998).

THEORY

Probabilistic and deterministic kinetic models

The experiment of the present method is designed to operate in such a way that adhesion appears as a random event, i.e., whether or not binding occurs in a particular adhesion test is nondeterministic, even when all conditions controllable by the experimenter, including the area (A_c) and duration (t) of contact between the two cells, as well as their respective surface densities of receptors (m_r) and ligands (m_l), are kept identical. It is hypothesized that such randomness is a manifestation of the stochastic nature inherent in the chemistry of receptor-ligand binding, which becomes significant when the number of bonds per cell is small. A single deterministic value (scalar) for the (averaged) surface density of bonds, $\langle n\rangle/A_c$, is no longer adequate for a complete description of the phenomenon, as the number of bonds that an adherent cell may have becomes a discrete, time-varying, random variable that fluctuates significantly. Instead, one considers a probability vector $\{p_0, p_1, \ldots, p_n, \ldots, p_{A_c m_{min}}\}$ to describe the state of the system. In other words, the adhesion could be mediated by any number of bonds ranging from 0 to $A_c m_{min}$, where $m_{min} = \min(m_r, m_l)$. Each possible scenario, say adherent via n bonds, has a defined likelihood, given by p_n.

For the experiment in question, there is no bond at the instant when the two cells are just brought into contact with each other ($t = 0$), so

$$p_n(0) = \begin{cases} 1 & \text{for } n = 0 \\ 0 & \text{for } n \neq 0. \end{cases} \tag{1}$$

Upon contact, bonds start to form, so $p_n(t)$ ($n > 0$) increases with time t. For a single step reversible reaction of ν_r receptors (designated M_r) binding to ν_l ligands (designated M_l) to form ν_b bonds (designated M_b), as given by the chemical reaction equation

$$\nu_r M_r + \nu_l M_l \underset{k_r^0}{\overset{k_f^0}{\rightleftarrows}} \nu_b M_b,$$

the master equations that govern the rates of change of these $A_c m_{min} + 1$ probability components can be written as

$$\frac{dp_n}{dt} = (n+1)^{\nu_b}\frac{k_r^0}{A_c^{\nu_b-1}}p_{n+1} - \left[\left(A_c m_r - \frac{\nu_r}{\nu_b}n\right)^{\nu_r}\left(A_c m_l - \frac{\nu_l}{\nu_b}n\right)^{\nu_l}\frac{k_f^0}{A_c^{\nu_r+\nu_l-1}} + n^{\nu_b}\frac{k_r^0}{A_c^{\nu_b-1}}\right]p_n \tag{2}$$

$$+ \left[A_c m_r - \frac{\nu_r}{\nu_b}(n-1)\right]^{\nu_r}\left[A_c m_l - \frac{\nu_l}{\nu_b}(n-1)\right]^{\nu_l}\frac{k_f^0}{A_c^{\nu_r+\nu_l-1}}p_{n-1},$$

where k_f^0 and k_r^0 are, respectively, the forward and reverse rate constants, of dimensions $[\text{area}]^{\nu_r+\nu_l-1}[\text{time}]^{-1}$ and $[\text{area}]^{\nu_b-1}[\text{time}]^{-1}$, respectively. The superscript 0 is used to indicate that these are rate constants measured under the condition that there is no external force applied to the bonds (see Discussion).

The above probabilistic master equations are generalization of the deterministic kinetic equation, as can be seen in the following derivation. Multiplying Eq. 2 by n/A_c and summing the resulting equation from 0 to $A_c m_{min}$ yields

$$\frac{d}{dt}\left(\frac{\langle n\rangle}{A_c}\right) = k_f^0\left[\left(m_r - \frac{\nu_r}{\nu_b}\frac{\langle n\rangle}{A_c}\right)^{\nu_r}\left(m_l - \frac{\nu_l}{\nu_b}\frac{\langle n\rangle}{A_c}\right)^{\nu_l} + \frac{\sigma_n^{(\nu_r+\nu_l)}}{A_c^{\nu_r+\nu_l}}\right] - k_r^0\left[\left(\frac{\langle n\rangle}{A_c}\right)^{\nu_b} + \frac{\sigma_n^{(\nu_b)}}{A_c^{\nu_b}}\right] \tag{3a}$$

where $\langle\ \rangle$ denotes averaging. $\langle n\rangle/A_c$ in Eq. 3a can readily be identified as corresponding to the deterministic density of bonds. The two measures of fluctuations in the bond number are

$$\sigma_n^{(\nu_r+\nu_l)} \equiv \sum_{i=0}^{\nu_r}\sum_{j=0}^{\nu_l}\binom{\nu_r}{i}\binom{\nu_l}{j} \cdot (A_c m_r)^{\nu_r-i}(A_c m_l)^{\nu_l-j}\left(-\frac{\nu_r}{\nu_b}\right)^i\left(-\frac{\nu_l}{\nu_b}\right)^j(\langle n^{i+j}\rangle - \langle n\rangle^{i+j}) \tag{3b}$$

and

$$\sigma_n^{(\nu_b)} \equiv \langle n^{\nu_b}\rangle - \langle n\rangle^{\nu_b}. \tag{3c}$$

It can readily be shown that $\sigma_n^{(\nu_b)} = 0$ when $\nu_b = 1$, $\sigma_n^{(\nu_r+\nu_l)} = 0$ when $\nu_r + \nu_l = 1$, $\sigma_n^{(\nu_b)} = \sigma_n^2$ when $\nu_b = 2$, and $\sigma_n^{(\nu_r+\nu_l)} = \sigma_n^2$ when $\nu_r = \nu_l = 1$, where σ_n^2 is the variance of n. For large systems, the fluctuations are small. Dropping $\sigma_n^{(\nu_r+\nu_l)}$ and $\sigma_n^{(\nu_b)}$ from Eq. 3a reduces it to the familiar deterministic kinetic equation, as expected.

Closed-form transient and steady-state solutions

Two simplified versions of Eq. 2 have been discussed in the literature. The first case is when one of the molecular species excessively outnumbers the other. Under such a condition the number of the former species [density $m_{max} = \max(m_r, m_l)$] in the free state can be approximated as constant in the contact area, as the reaction is limited by the availability of the latter species (density m_{min}). The $\nu_r = \nu_l = \nu_b = 1$ case of such a simplified version of Eq. 2 was used by Cozens-Roberts et al. (1990) when they first applied the probabilistic kinetic formulation of McQuarrie (1963) to the analysis of receptor-ligand binding. We were able to find closed-form solutions to this case, provided that the kinetic rates are constants, which they are in the present case. The solution that satisfies the initial condition given by Eq. 1 is of

the form of the binomial distribution (see Appendix):

$$p_n(t) = \binom{A_c m_{min}}{n} [p(t)]^n [1 - p(t)]^{A_c m_{min} - n}, \qquad (4a)$$

where $p(t)$ is the probability of forming one bond, given by

$$p(t) = \frac{1 - \exp(-kt)}{1 + (m_{max} K_a^0)^{-1}}. \qquad (4b)$$

The two parameters, $K_a^0 = k_f^0/k_r^0$ and $k = m_{max} k_f^0 + k_r^0$, are the equilibrium association constant (binding affinity) and the overall rate (reciprocal time scale) of the reaction, respectively.

The second case is that in which the number of bonds that have nonvanishing probabilities is much smaller than the numbers of receptors and ligands. Under such a condition the formation of a small number of bonds will not significantly deplete the free receptors and ligands available in the contact area, so Eq. 2 can be approximated by one that neglects, respectively, n and $(n - 1)$ in the $[A_c m_j - (\nu_j/\nu_b)n]$ and $[A_c m_j - (\nu_j/\nu_b)(n - 1)]$ (subscript $j = r$ or l) terms. Such simplified master equations (with variable kinetic rates) have been discussed by Long et al. (manuscript submitted for publication). The $\nu_b = 1$ case (with constant kinetic rates) was employed by Kaplanski et al. (1993), who solved the equations numerically. (Different notations, $k_+ = A_c m_r^{\nu_r} m_l^{\nu_l} k_f^0$ and $k_- = k_r^0$, were used by Kaplanski et al. (1993). The analytical solution we found (see Appendix) is of the form of the Poisson distribution:

$$p_n(t) = \frac{\langle n \rangle^n}{n!} \exp(-\langle n \rangle), \qquad (5a)$$

where $\langle n \rangle$ is the average number of bonds, given by

$$\langle n \rangle = A_c m_r^{\nu_r} m_l^{\nu_l} K_a^0 [1 - \exp(-k_r^0 t)]. \qquad (5b)$$

These results are not surprising, as the assumptions on which Eq. 2 and its two simplified versions (Eqs. A1 and A11) are based are equivalent, respectively, to those underlying the binomial and Poisson distributions. Both distributions have been suggested to describe the formation of a small number of bonds (Capo et al., 1982; Chesla et al., 1995; Evans and Ritchie, 1994). However, in contrast to the previous works that assumed p and $\langle n \rangle$ given a priori, our closed-form solutions provide their explicit expressions, Eqs. 4b and 5b.

Although an explicit transient solution to Eq. 2 in the form similar to that of Eq. 4 or 5 for arbitrary ν_r, ν_l, and ν_b values has not been found, implicit solution can be obtained by assuming $\{p_n(t)\} = \{A_n\}e^{rt}$ to convert the problem of solving $A_c m_{min} + 1$ coupled, first-order, constant coefficient, ordinary differential equations to one of finding the eigenvalues r and eigenvectors $\{A_n\}$ of the corresponding linear algebraic system (Boyce and DiPrima, 1977).

At steady state, explicit exact solutions for Eq. 2 and its two simplified versions have been obtained for arbitrary stoichiometric coefficients (Zhu et al., 1998). These steady-state solutions, derived by using mathematical induction (Piper, 1997), are, respectively:

$$p_n(\infty) = \begin{cases} \left\{ \sum_{m=0}^{A_c m_{min}} (m!)^{\nu_r + \nu_l - \nu_b} \left[\binom{\frac{\nu_b}{\nu_r} A_c m_r}{m} \right]^{\nu_r} \left[\binom{\frac{\nu_b}{\nu_l} A_c m_l}{m} \right]^{\nu_l} \cdot \left[\left(\frac{\nu_r}{\nu_b}\right)^{\nu_r} \left(\frac{\nu_l}{\nu_b}\right)^{\nu_l} \frac{K_a^0}{A_c^{\nu_r + \nu_l - \nu_b}} \right]^m \right\}^{-1} & n = 0 \\ p_0(\infty)(n!)^{\nu_r + \nu_l - \nu_b} \left[\binom{\frac{\nu_b}{\nu_r} A_c m_r}{n} \right]^{\nu_r} \left[\binom{\frac{\nu_b}{\nu_l} A_c m_l}{n} \right]^{\nu_l} \cdot \left[\left(\frac{\nu_r}{\nu_b}\right)^{\nu_r} \left(\frac{\nu_l}{\nu_b}\right)^{\nu_l} \frac{K_a^0}{A_c^{\nu_r + \nu_l - \nu_b}} \right]^n & n > 0 \end{cases} \qquad (6)$$

$$p_n(\infty) = \begin{cases} \left\{ \sum_{m=0}^{A_c m_{min}} (m!)^{\nu_i - \nu_b} \left[\binom{\frac{\nu_b}{\nu_i} A_c m_{min}}{m} \right]^{\nu_i} \left[\left(\frac{\nu_i}{\nu_b}\right)^{\nu_i} \frac{m_{max}^{\nu_a} K_a^0}{A_c^{\nu_i - \nu_b}} \right]^m \right\}^{-1} & n = 0 \\ p_0(\infty)(n!)^{\nu_i - \nu_b} \left[\binom{\frac{\nu_b}{\nu_i} A_c m_{min}}{n} \right]^{\nu_i} \left[\left(\frac{\nu_i}{\nu_b}\right)^{\nu_i} \frac{m_{max}^{\nu_a} K_a^0}{A_c^{\nu_i - \nu_b}} \right]^n & n > 0 \end{cases} \qquad (7)$$

and

$$p_n(\infty) = \begin{cases} \left[\sum_{m=0}^{\infty} \frac{(A_c^{\nu_b} m_r^{\nu_r} m_l^{\nu_l} K_a^0)^m}{(m!)^{\nu_b}} \right]^{-1} & n = 0 \\ p_0(\infty) \frac{(A_c^{\nu_b} m_r^{\nu_r} m_l^{\nu_l} K_a^0)^n}{(n!)^{\nu_b}} & n > 0, \end{cases} \qquad (8)$$

where $\nu_a = \nu_r$ and $\nu_i = \nu_l$ if $m_{max} = m_r$, but $\nu_a = \nu_l$ and $\nu_i = \nu_r$ when $m_{max} = m_l$. Note that as $t \to \infty$, Eqs. 4 and 5 approach, respectively, the $\nu_r = \nu_l = \nu_b = 1$ case of Eq. 7 and the $\nu_b = 1$ case of Eq. 8, as expected.

These explicit exact steady-state solutions, Eqs. 6–8, are of interest because they greatly facilitate the test of the validity of the binomial and Poisson solutions, Eqs. 4 and 5. As one might expect from physical intuition, the discrepancies between the binomial and Poisson approximate solutions and the solution to the original master equations, Eq. 2, are at maximum at steady state because this is when the average bond number reaches maximum. Thus the discrepancies between the steady-state solutions, Eqs. 6 and 7 (or Eqs. 6 and 8), represent the worse-case scenario for all time-dependent solutions. The results of the validity test are shown in Fig. 2, in which the $p_0(\infty)$ ratio of the solution to the simplified version to the solution to the full master equations is plotted against either m_{max}/m_{min} (Fig. 2 *A*) or $(\nu_b/\nu_i)A_c m_{min}/\langle n \rangle_\infty$ (Fig. 2 *B*). It can be seen that, when m_{max}/m_{min} [or $(\nu_b/\nu_i)A_c m_{min}/\langle n \rangle_\infty$] is on the order of one, Eq. 7 (or 8) differs significantly from Eq. 6, suggesting the breakdown of the binomial (or Poisson) type of approxima-

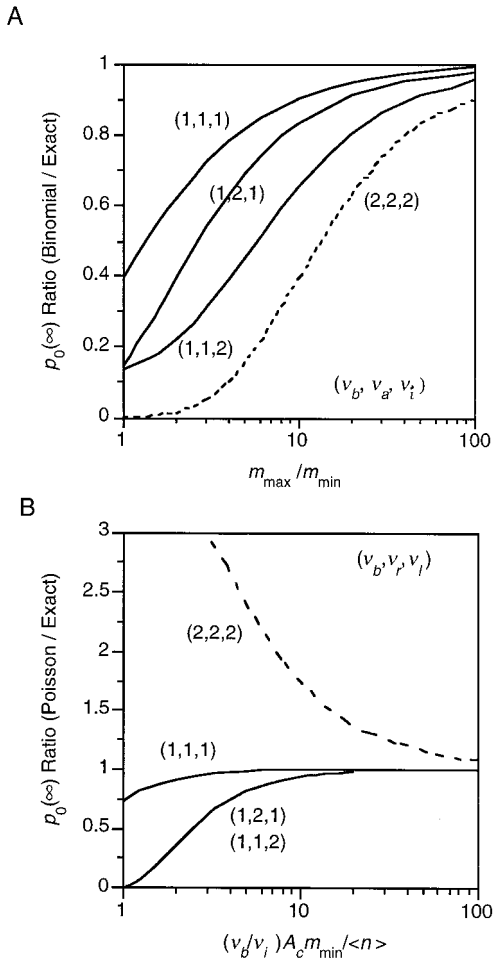

FIGURE 2 Validation of the two simplified master equations in approximating the full master equations. The ratios to the full steady-state solution (Eq. 6) of the binomial-type steady-state solution (Eq. 7) (*A*), and the Poisson-type steady-state solution (Eq. 8) (*B*) are plotted against the parameters m_{max}/m_{min} for the binomial-type solution and $(\nu_b/\nu_i)A_c m_{min}/\langle n \rangle$ for the Poisson-type solution, respectively, that control the validity of the corresponding approximation. Different curves represent different stoichiometric coefficients (ν_b, ν_r, ν_l), as indicated. Note that the experimental conditions in the present work satisfy $[(\nu_b/\nu_i)A_c m_{min}/\langle n \rangle] > 100$, which is in the parameter range that validates the two types of approximation.

tion. However, as m_{max}/m_{min} [or $(\nu_b/\nu_i)A_c m_{min}/\langle n \rangle_\infty$] increases to more than 50, the $p_0(\infty)$ ratio quickly approaches unity, supporting the validity of the solution to the simplified master equations in approximating the solution to the full equations in these parameter domains, which correspond to the conditions of the present experiment.

RESULTS

Quantification of receptor and ligand surface densities

The quantification of surface densities of CD16A expressed on CHO cells and IgG coated on RBC is illustrated in Fig. 3. Fig. 3 *A* shows the results of one of the radioimmunoassays (Scatchard plot) used to quantify the receptor density. Fig. 3 *B* shows the receptor expression in samples of the same CHO cells measured by flow cytometry with calibration beads. As can be seen in Fig. 3 *C*, the receptor densities determined via the two methods are comparable. Flow cytometric analysis was solely used to determine the ligand densities on RBCs (Fig. 3 *D*).

Measurement of the adhesion probability

The measurement of adhesion probability per contact is illustrated in Fig. 4, in which the running averages (adhesion frequency) of the binary adhesion scores (one if adhesion results, and zero if not) for sequential adhesion tests are plotted against the test cycle count. Not only were the same pair of cells used in each set of repeated tests, but the location, area, and duration of all of the contacts in the same sequence were also kept constant by the experimenter. Thus the fluctuations in the running frequencies, especially at low test cycle counts, were most likely due to the randomness inherent to small system kinetics of receptor-ligand binding. The running adhesion frequencies became stabilized as the test number increased, allowing the adhesion probability, P_a, to be estimated from the adhesion frequency (see Fig. 4 legend). To ensure statistically stable results, at least 400 repeated tests were conducted for each data point, using multiple cell pairs. A total of ~7250 single cell pair adhesion tests were performed to yield the data presented in this paper.

Demonstration of binding specificity

Also shown in Fig. 4 is the fact that coating an irrelevant protein (BSA) instead of the ligands on the RBCs resulted in a dramatic decrease in the adhesion probability. The binding specificity is further demonstrated in Fig. 5, which summarizes the results of experiments designed to address this question. As can be seen from Fig. 5 *A*, under the same contact duration (5 s) and apparent area (3 μm^2), hIgG-coated RBCs adhered with high probability to CHO cells transfected to express CD16A, but not to untransfected parental CHO cells (K1) or to CHO cells (A5) transfected with an irrelevant receptor (integrin $\alpha_{IIb}\beta_3$). Moreover, CD16A-expressing CHO cells did not adhere to uncoated RBCs or RBCs coated with an irrelevant protein (BSA). In addition, the adhesion probabilities were reduced to the nonspecific level of binding when the CD16A-expressing CHO cells were preincubated with the adhesion-blocking anti-CD16 monoclonal antibody (mAb) (CLB at 10 μg/ml), or when the hIgG-coated RBCs were preincubated with a soluble CD16A molecule (Li et al., manuscript in preparation). By contrast, preincubation of the CD16A-expressing CHO cells with an irrelevant mAb (X63) or of the hIgG-coated RBCs with an irrelevant soluble molecule (B7) had no effect (Fig. 5 *B*). These data established that the measured cell adhesions were mediated by the specific interactions between CD16A and hIgG.

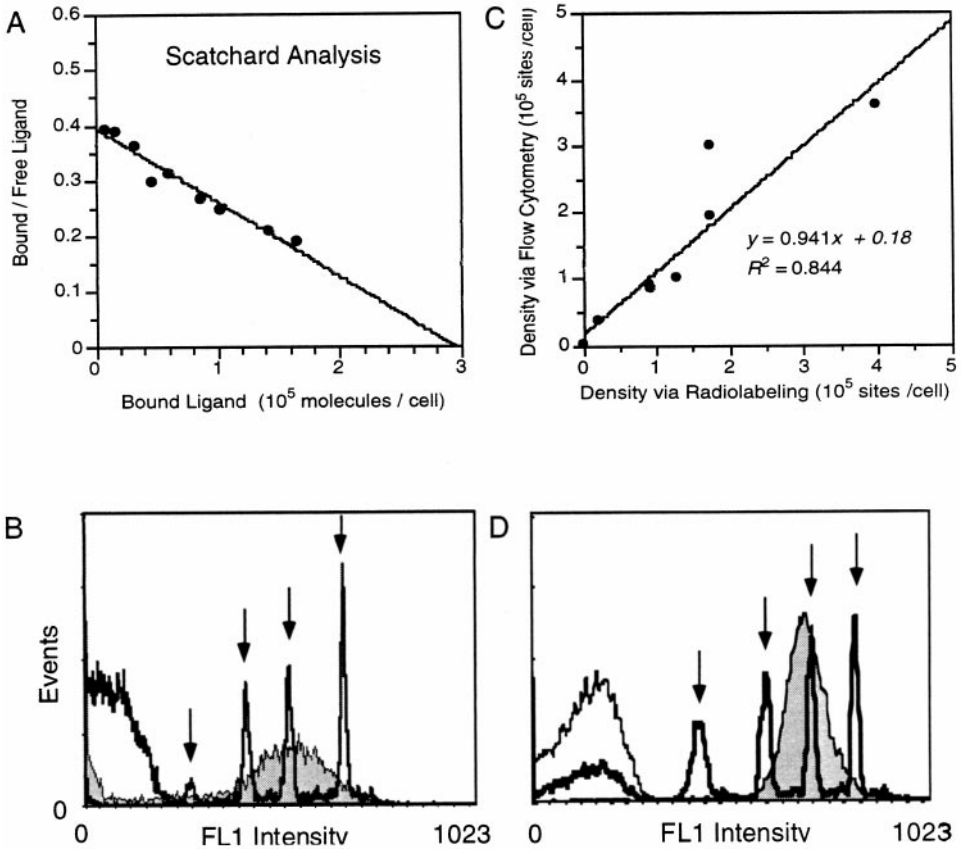

FIGURE 3 Quantification of molecular density on the cell surface. (*A*) The radioimmunoassay method involves radiolabeling specific antibodies against the membrane protein and determining its density by counting the amount of antibody bound to the cell surface as it varies with the concentration of antibodies added in the solution. The *x* intercept of the Bound/Free versus Free line in the Scatchard plot predicts the total number of receptors per cell, where B and F denote, respectively, the fractions of antibody that are bound to the cell and free in the solution. (*B*) The flow cytometer method is similar, except that the cell labeling is accomplished in a two-step process with the secondary antibody fluorescently tagged. The distributed fluorescent intensity of the CD16A+ cells (*shaded curve*) is then compared to those of the standard calibration beads (*four unshaded curves, arrows*). The negative control (without primary antibody) (*unshaded curve near origin*) is shown for comparison. (*C*) Comparison between receptor densities determined by the two methods, using sorted CHO cells expressing various narrow levels of CD16A (*points*). A strong correlation can be seen from the linear fit of the data (*line*). (*D*) Determination of IgG site density on RBCs, as in (*B*).

Dependence of adhesion probability on contact duration

It can also be seen in Fig. 4 that, when the contact times in a test sequence were prolonged from 5 to 10 s, the adhesion probability was increased. The dependence of P_a on t was systematically measured; the results (after subtracting the nonspecific binding) are shown in Fig. 6. As expected, the adhesion probability increased with increasing contact duration initially and then reached a plateau. The initial transient phase contains information about kinetic rates, whereas the equilibrium association constant can be derived from the steady state. Furthermore, for fixed contact durations, P_a increased with both the densities of the receptor and the ligand, as expected from the law of mass action.

Because $P_a(t) = 1 - p_0(t)$ is also solved from the master equations, comparing the measured and the predicted dependence of adhesion probability on contact time allows us to evaluate the kinetic rates. However, rate constants so calculated represent intrinsic properties if and only if the correct kinetic mechanism, i.e., the realistic order of the reaction, is assumed in Eq. 2. To identify the appropriate kinetic mechanism, the ability of the theory to account for the experiment was compared with the different stoichiometric coefficients assumed.

Determination of the kinetic mechanism

We first examine the order of dissociation. The Poisson type of simplified master equations was used to address this question, because the valences of the receptor and the ligand, ν_r and ν_l, need not be specified for such a case, as they are lumped into one of the two curve-fitting parameters, $A_c m_r^{\nu_r} m_l^{\nu_l} k_f^0$ and $A_c^{1-\nu_b} k_r^0$. The equations were solved for various ν_b values, and the errors between the predictions and the data were minimized by adjusting the lumped rate parameters for each of the four P_a versus t curves in Fig. 6. The minimum χ^2 (averaged over four curves) is plotted in

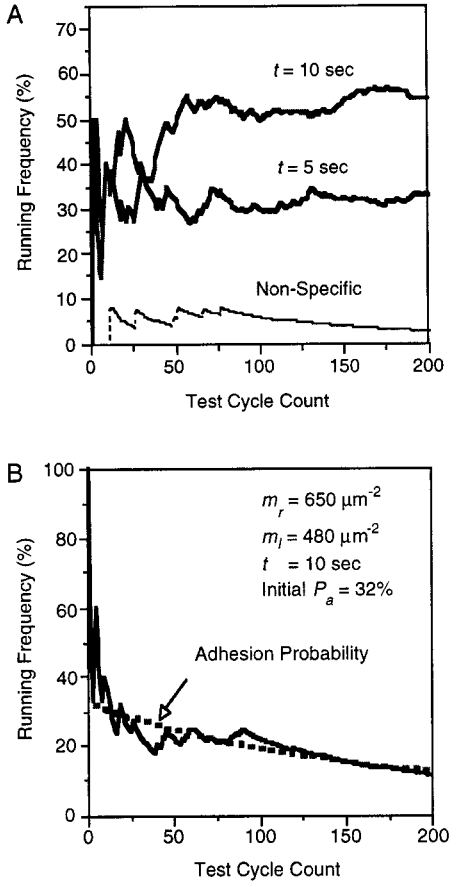

FIGURE 4 Measurement of adhesion probability per contact. (*A*) The running averages of adhesion scores versus test cycle counts of three sequences of 200 adhesion tests each, each performed in a single cell pair of a CD16A-expressing CHO cell (m_r = 650 μm^{-2}) interacting with a RBC coated with either human IgG (m_l = 1200 μm^{-2}, *solid curves*) or BSA (*dashed curve*). The apparent contact area was kept constant (~3 μm^2) for all tests. The contact durations were t = 5 s for the BSA (nonspecific) and one of the hIgG-coated test series and t = 10 s for the other hIgG-coated series, as indicated. The adhesion probability for each cell pair was estimated from the running adhesion frequency at the last adhesion test (54% and 35% for CD16-hIgG, 10- and 5-s contact durations, respectively, and 3% for CD16-BSA, 5-s contact time). The specificity of the adhesions is seen from the dependence of adhesion probability on the presence of hIgG on the RBC surface. The feasibility of measuring adhesion kinetics is revealed from the dependence of adhesion probability on contact time. The stability of the running adhesion frequency after 50 test cycles is an indication of its adhesive detachment mechanism (receptor-ligand dissociation). (*B*) Illustration of another type of running adhesion frequency (*solid curve*), this time declining with increasing test cycle counts, which suggests a cohesive detachment mechanism (molecular extraction from the cell membrane). This type of irreversible behavior was found when the coated ligand was a specific antibody against the receptor (anti-CD16 mAb Leu-11b). The adhesion probability (*dotted curve*), determined by fitting of the entire running adhesion frequency curve to a Markov process model (Chesla et al., manuscript in preparation), decreases with the test cycle count, suggesting the gradual loss of functioning adhesion molecules in the contact area. Its extrapolated initial value before the first test (32%) can be used for the purposes of the present method.

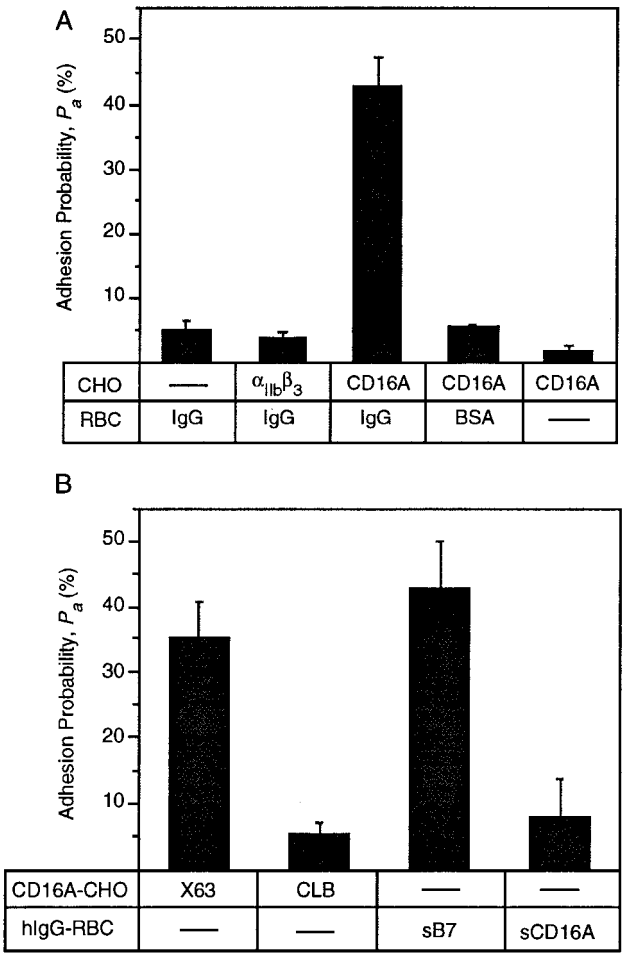

FIGURE 5 Demonstration of binding specificity. (*A*) The adhesion probability varied with the molecular combinations present or absent on the apposing cell surfaces. When CD16A was expressed on the CHO cell and the RBC was coated with hIgG, a high adhesion probability (45%) was observed. In contrast, when either no receptor (−) or an irrelevant receptor ($\alpha_{IIb}\beta_3$) was expressed on the CHO cell, low adhesion probabilities (5% and 4%, respectively) were observed for the same hIgG coating on the RBC. Similarly, when no ligand (−) or an irrelevant protein (BSA) coated the RBC, the adhesion probability was reduced to low levels (6% and 2%, respectively) for the same CD16A-expressing CHO cells. (*B*) The adhesion could also be inhibited by incubating the cells with blocking agents. The addition of the conditioned medium of hybridoma secreting anti-CD16 mAb CLB (contained ~10 μg/ml antibody) reduced the adhesion probability to 5%. Similarly, the addition of the conditioned medium of soluble CD16A-secreting CHO cells (contained ~10 μg/ml sCD16A) decreased the adhesion probability to 8%. In contrast, conditioned media of hybridoma secreting an irrelevant mAb X63 and of CHO cells secreting an irrelevant soluble molecule B7 had no effect on the overall adhesion probability (35% and 42%, respectively). Each of the bars in *A* and *B* represents mean ± standard error of data from two to four series of 50–200 tests, each at a contact duration of 5 s.

Fig. 7 *A* against the ν_b value. It appears that the reverse reaction is of the first order, as this mechanism (ν_b = 1) is best able to reproduce the data (i.e., results in the lowest χ^2).

The above conclusion that the CD16A-hIgG interaction obeys first-order dissociation greatly facilitated the remaining investigation for the kinetic mechanism, as the closed-form solution, Eq. 5, can now be applied to the data analysis. Not only is this handy to use, but it also suggests informative ways of presenting the data for hypothesis

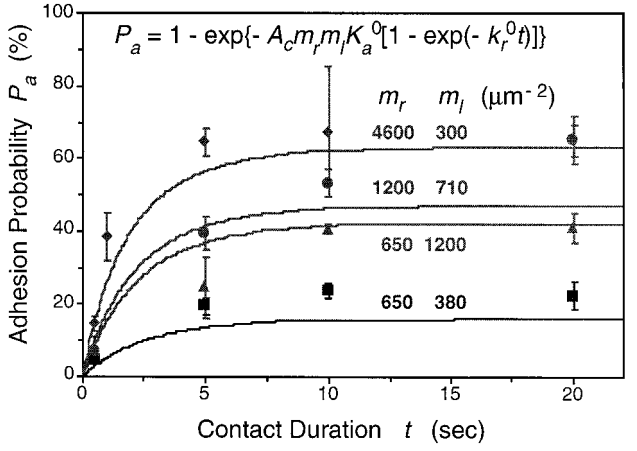

FIGURE 6 Dependence of adhesion probability on contact time and densities of receptors and ligands. The total adhesion probability (P_t), measured as described in Fig. 4, was converted into the probability of specific adhesion P_a (= $(P_t - P_n)/(1 - P_n)$, where the probability of nonspecific adhesion P_n was P_t at $m_l = 0$, i.e., measured with BSA-coated RBC), plotted as a function of the contact duration for each set of receptor and ligand densities, and fitted with the indicated theoretical solution (*curves*). A single set of kinetic rate constants (listed in Table 1) was used to fit all data corresponding to four different pairs of (m_r, m_l) values (indicated). The data (*points*) represent mean ± standard error of two to five series of tests of at least 50 each to yield at least 400 total tests per data point.

testing. It follows from Eq. 5 that

$$\ln[\ln(1 - P_a)^{-1}] = \nu_r \ln m_r + \nu_l \ln m_l + \ln\{A_c K_a^0[1 - \exp(-k_r^0 t)]\}. \quad (9)$$

Thus, in $\ln[\ln(1 - P_a)^{-1}]$ versus $\ln m_l$ (or $\ln m_r$) plots, the data should appear as linear for each fixed t and m_r (or m_l), and the slope of the line should be the valence of the ligand, ν_l (or the receptor, ν_r). To test this argument, the two sets of P_a versus t data shown in Fig. 6 that correspond to the same m_r (= 652 μm^{-2}) were replotted in Fig. 8 *A* as $\ln[\ln(1 - P_a)^{-1}]$ versus $\ln m_l$ for various t. It can be seen that, as the contact time changes, the y intercept of the $\ln[\ln(1 - P_a)^{-1}]$ versus $\ln m_l$ line shifts, but its slope remains nearly the same (= 0.86 for the average of four constant time lines). Because ν_l can only take positive integer values, the data suggest that hIgG is a monovalent ligand for CD16A.

We can now use the conclusion of $\nu_l = 1$ to subtract the term involving the ligand on the right-hand side of Eq. 9. This allowed us to plot $\ln[\ln(1 - P_a)^{-1}] - \ln m_l$ versus $\ln m_r$ in Fig. 8 *B*, using all four sets of P_a versus t data. It is evident that, for each fixed contact time, the data appear to line up in a straight line with a slope of approximately unity. Not only does this indicate the monovalency of CD16A binding; it also supports the validity of the present method for determining the kinetic mechanism. Further support of this argument is provided in Fig. 7 *B*, in which the minimum χ^2 is plotted against ν_r and ν_l. A single set of kinetic rates, $A_c k_f^0$ and k_r^0, were used to fit all P_a versus t data for each pair of ν_r and ν_l values for all admissible ν_b [$\leq \min(\nu_r, \nu_l)$]

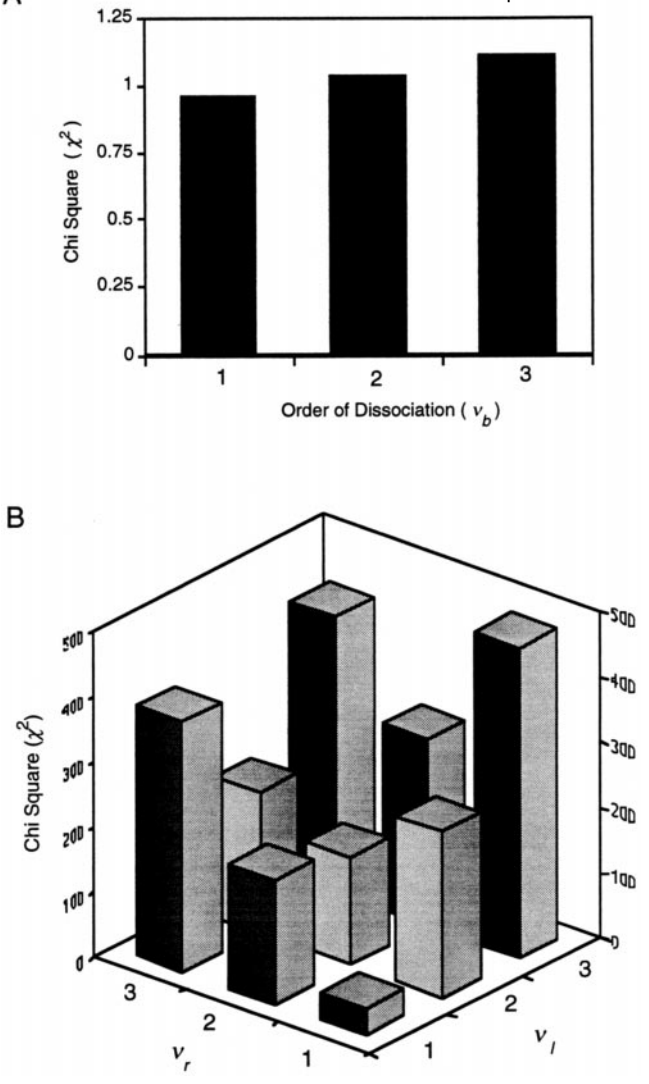

FIGURE 7 Comparison of the abilities of various kinetic mechanisms to account for the data. (*A*) The solutions of the Poisson-type master equations with various orders of dissociation (ν_b) were fitted separately to each of the four sets of P_a versus t data from Fig. 6. The sum of squared weighted errors (χ^2) from all of the curves was averaged and plotted against the ν_b value. (*B*) The four sets of data from Fig. 6 were simultaneously fitted by the solutions of the full master equations (Eq. 2), with various stoichiometric coefficients, ν_b, ν_r, and ν_l. The minimum χ^2 was calculated as a function of ν_r and ν_l. At each pair of (ν_r, ν_l) values, the lowest χ^2 for all admissible ν_b ($\leq \min(\nu_r, \nu_l)$) values was plotted (*bars*).

values. Again, the bimolecular binding mechanism between a single epitope on CD16A and a single binding site on the Fc domain of hIgG ($\nu_r = \nu_l = 1$) was bound to be best able to describe the data. This conclusion further supports the first-order dissociation mechanism, as ν_b cannot be greater than the smaller of ν_r and ν_l.

Validating the theoretical predictions and evaluating the kinetic rate constants

It follows from Eq. 9 that, when $\nu_r = \nu_l = 1$ and for a fixed value of t, $\ln(1 - P_a)^{-1}$ should increase bilinearly with m_r

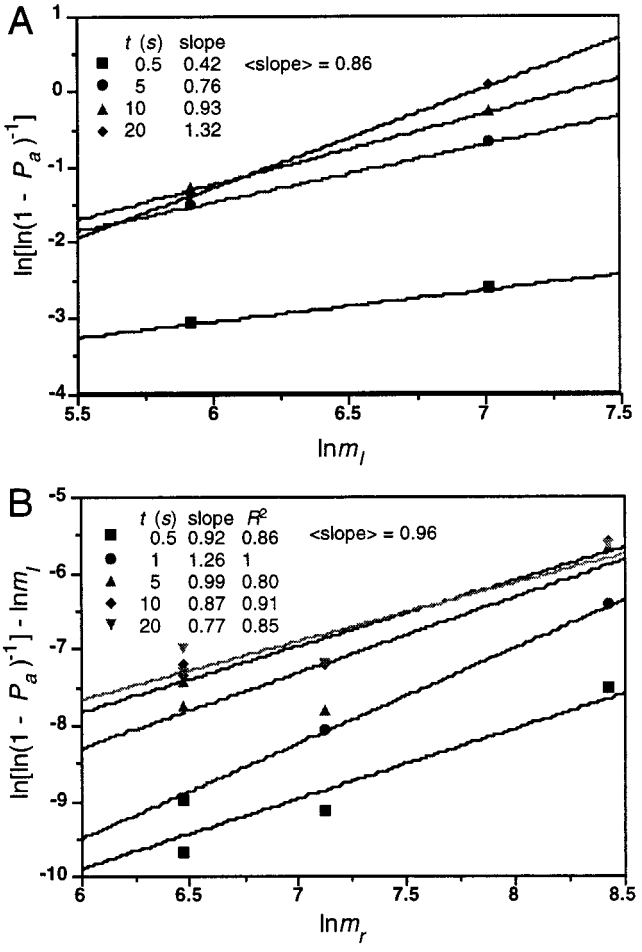

FIGURE 8 Demonstration of the monovalency of CD16A-hIgG binding. (*A*) The two P_a versus t curves from Fig. 6 that correspond to the same receptor expression level (m_r = 650 μm^{-2}) but different ligand coating densities (m_l = 380 and 1200 μm^{-2}) were replotted as $\ln[\ln(1 - P_a)^{-1}]$ versus $\ln m_l$ data (*points*) for each contact duration t (indicated) and fitted with a linear function (*lines*). The nearest integer of the slopes of these lines (indicated) is predicted to be the most probable value of ν_l, which is 1. (*B*) All curves from Fig. 6 were replotted as $\ln[\ln(1 - P_a)^{-1}] - \ln m_l$ versus $\ln m_r$ data (*points*) for each contact duration t (indicated) and fitted with a linear function (*lines*) with the goodness of fit indicated by the R^2 value. The nearest integer of the slopes of these lines (indicated) is predicted to be the most probable value of ν_b, which again is unity.

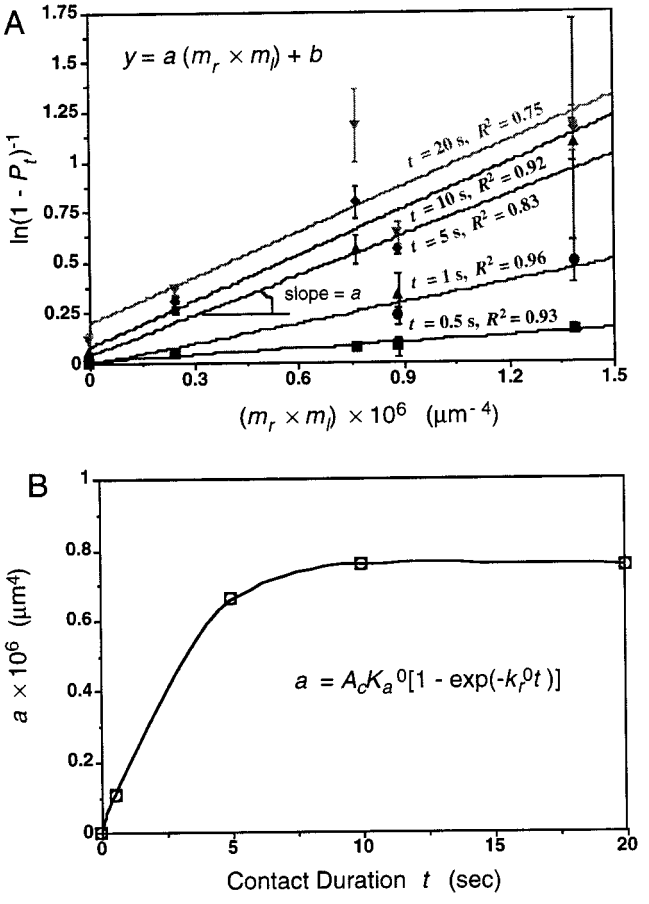

FIGURE 9 Further demonstration of the bimolecular kinetic mechanism. (*A*) The probability of total adhesion P_t versus the product of surface densities ($m_r \times m_l$) of CD16A and hIgG is shown in a semilog plot ($P_t \approx \ln(1 - P_t)^{-1}$ for small P_t). For each contact duration t (indicated), the data (*points*) were fitted with a linear function (*lines*), and the goodness of fit was indicated by the R^2 value. The error bars were computed from the original data according to the Gaussian error propagation law. (*B*) The slopes of the individual lines from (*A*) were plotted against t and fitted with the indicated equation. The ability of the theoretical model to fit the data well in both panels is another indication that the proper kinetic mechanism is being assumed, i.e., $\nu_r = \nu_l = \nu_b = 1$.

and m_l. The slope of the $\ln(1 - P_a)^{-1}$ versus $m_r \times m_l$ line should be equal to $A_c K_a^0[1 - \exp(-k_r^0 t)]$. These predictions were tested in Fig. 9 and were found to be well supported by the data. Minimizing the errors between the predicted and measured slope versus contact time relationship (Fig. 9 *B*) makes it possible to evaluate the binding affinity (per contact area), $A_c K_a^0$, and the reverse rate constant, k_r^0. To test the accuracy and reliability of these values, the kinetic rate constants were also calculated using each P_a versus t curve in Fig. 6 for various m_r and m_l levels, as well as fitting all of the data simultaneously (Table 1). Conversely, the k_f^0 and k_r^0 values evaluated from the fitting of one P_a versus t curve were then used to predict other P_a versus t curves obtained from independent experiments using different levels of m_r and m_l (not shown). The ability of the model to use only a single pair of rate constants to fit a wide range of data, including five time points and four ligand and three receptor densities, not only attests to the validity of the method employed, but also suggests that the estimated parameters are indeed intrinsic molecular properties.

Additional support for the theory was found when it was tested for the predicted functional form of the adhesion probability, i.e., that all P_a versus t data for the same receptor-ligand pair should collapse into a single $(m_r m_l)^{-1}\ln(1 - P_a)^{-1}$ versus t curve, regardless of the densities of the receptors and ligands (Fig. 10). The four P_a versus t curves shown in Fig. 6 did indeed collapse in Fig. 10. When the origin of the IgG ligands was changed from human to rabbit, the $(m_r m_l)^{-1}\ln(1 - P_a)^{-1}$ versus t curve shifted, indicating different kinetic rate constants for different molecular pairs. Indeed, human CD16A binds twice as

TABLE 1 Summary of kinetic rate constants

IgG origin	m_r (μm^{-2})	m_l (μm^{-2})	$A_c k_f^0 \times 10^7$ ($\mu m^4\ s^{-1}$)	k_r^0 (s^{-1})	$A_c K_a^0 \times 10^6$ (μm^4)
Human	650	380	4.0 ± 1.5	0.36 ± 0.16	1.1
Human	650	1200	1.9 ± 3.7	0.13 ± 0.06	1.4
Human	1200	710	2.5 ± 0.94	0.42 ± 0.18	0.59
Human	4600	300	2.9 ± 0.52	0.35 ± 0.09	0.82
Human	Combined data		2.6 ± 0.32	0.37 ± 0.06	0.72
Rabbit	1200	190	6.0 ± 0.42	0.25 ± 0.07	2.4
Rabbit	1200	360	5.2 ± 0.49	0.16 ± 0.05	3.3
Rabbit	Combined data		5.7 ± 0.31	0.20 ± 0.04	2.8

rapidly to, but dissociates half as rapidly from, rIgG than hIgG, leading to a fourfold difference in affinity (Table 1), which is consistent with the affinity difference measured when the IgGs were in solution (i.e., 3-D affinity; data not shown).

A simple graphic representation

Finally, we describe a simple graphic representation for estimation of the kinetic rates from the adhesion probability versus contact time data without using χ^2 fitting of nonlinear curves. The value of $A_c K_a^0$ can be estimated directly from the slope of the $\ln[1 - P_a(\infty)]^{-1}$ versus $m_r m_l$ plot, where $P_a(\infty)$ is the steady-state value of the adhesion probability. This has been exemplified in Fig. 9 (the 10- and 20-s lines in Fig. 9 *A* or the corresponding points in Fig. 9 *B*). Similarly, the value for the reverse rate constant can be estimated directly from the time, t_{50}, that is required for the P_a versus t data to achieve half-maximum,

$$k_r^0 = \frac{\ln 2}{t_{50}} C(A_c m_r m_l K_a^0), \tag{10a}$$

where C varies between 0 and 1; and its weak dependence on $A_c m_r m_l K_a^0$ can be derived from Eq. 5:

$$C = \frac{1}{\ln 2}\ln\,(1 + \{\ln[1 + \exp(-A_c m_r m_l K_a^0)] - \ln 2\}/(A_c m_r m_l K_a^0))^{-1}. \tag{10b}$$

As can be seen from Fig. 11, for the values of $A_c m_r m_l K_a^0$ encountered in the present work (cf. Table 1), C only varies between 0.7 and 0.9. Thus,

$$k_r^0 \approx t_{50}^{-1} \times 50\%. \tag{10c}$$

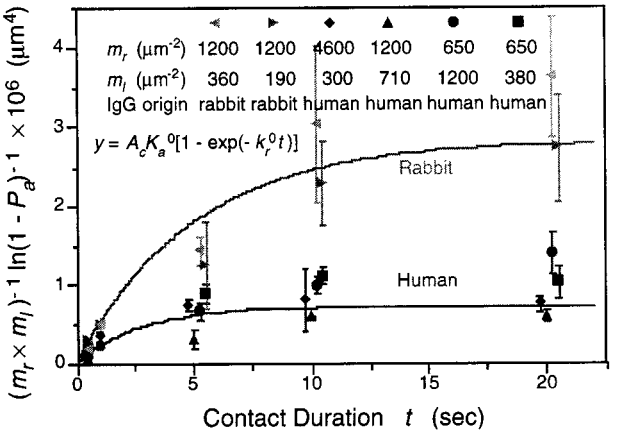

FIGURE 10 Validation of the functional form of the theoretical prediction. Data (*points*) from Fig. 6 (hIgG group) plus those measured for IgG from a different species (rabbit) were converted into a logarithmic scale, divided by ($m_r \times m_l$), plotted against t, and fitted with the indicated equation (*curves*). The theoretical solution predicts that, for the same receptor-ligand pair, data measured using different m_r and m_l values (indicated) should collapse into a single curve in this plot. Thus the difference in the two data groups reveals different kinetic rate constants for CD16A binding IgG of different origins (human and rabbit). As such, a single set of $A_c k_f^0$ and k_r^0 (cf. Table 1) was used to fit multiple data curves for the same receptor and ligand pair (CD16A-hIgG or CD16A-rIgG). The error bars were computed from the original data, using the Gaussian error propagation law. Adhesions were measured at t = 0.5, 1, 5, 10 and 20 s. However, not all data were plotted at the exact time points, to avoid symbol overlap.

DISCUSSION

The method measures zero-force rate constants

The goal of the present work was to develop a method to measure 2D kinetic rates when both of the interacting molecular species are anchored to apposing surfaces, as in the case of cell adhesion. An interesting feature of this method is that the chemistry of receptor-ligand binding is quantified

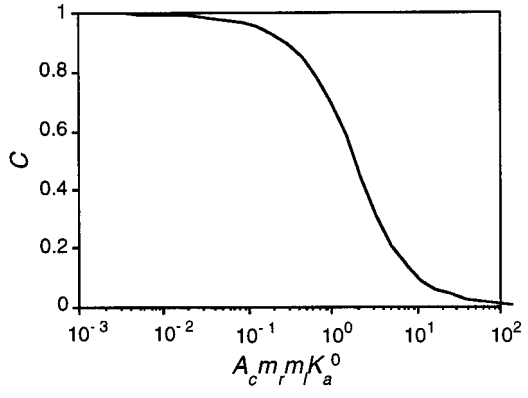

FIGURE 11 Value of C as given in Eq. 10, and its variation with $A_c m_r m_l K_a^0$.

mechanically. Because it is well known that applied forces can influence the binding kinetics (Bell, 1978), the question naturally arises: At what force level were the kinetic rates measured by the present method? The answer is that k_f^0 and k_r^0 represent rate constants at zero force, as indicated by their superscript. This is a critical contention, for without it, all of the analytical solutions to the master equations would have no longer been valid (cf. Long et al., manuscript submitted for publication; Piper et al., 1998).

The reason for the above contention is that, during the contact period, the pipette impingement force that pushes the two cells together is most likely borne by the membrane and/or cytoskeleton support rather than by the receptor-ligand bonds. Although at the end of the contact period the bonds (if adhesion occurs) are stretched and broken as the cells are being pulled apart, this only serves to provide a signal to the observer of whether or not adhesion occurred during the given contact time. It is necessary to apply force to break all bonds for the adhesion test to be repeated in the next cycle; but this takes place at a later time. The contact period ends at the instant when the piezo-driven pipette starts to pull the cells apart. Moreover, care was taken to ensure that the rate of force application was sufficiently fast that the time it took to break the contact was negligible compared to the shortest contact duration tested (see below). In other words, in the present method, one counts the occurrence of adhesion events in the contact time when no tensile force is applied, instead of measuring the time required for the forced dissociation of the preformed bonds in the postcontact adhesion-detection phase. The latter measurement, i.e., lifetime of stressed bonds, also contains kinetic information; and this is similar to the flow chamber experiment (Alon et al., 1995, 1997; Chen et al., 1997). Data obtained from this phase of the experiment and the mathematical model for their analyses will be described elsewhere (Zhu et al., manuscript in preparation). Thus, despite the fact that the formation of adhesive bonds can only be detected when they are broken by externally applied forces, the rates measured by the present method are those of spontaneous reaction in the absence of force.

The method measures receptor-ligand binding, not molecular extraction from the membrane

A useful extension from the above line of reasoning is that our protocol ensures that the measured rate constants represent the kinetics of reversible binding of receptors and ligands rather than their irreversible extraction from the cell membrane. The latter possibility always arises when the assay involves cell detachment (Evans et al., 1991). We have recently developed a novel method of addressing this question quantitatively. Although the details of this approach will be described elsewhere, the key observation is that the binding evolution curves such as those exemplified in Fig. 4 exhibit two qualitatively different features (Chesla et al., manuscript in preparation). One is characterized by the evenly distributed positive adhesion scores among all tests and a stable running frequency as the test cycle count becomes large (Fig. 4 *A*). The other is characterized by the concentration of positive adhesion scores in the earlier tests and a declining running frequency with increasing test cycle count (Fig. 4 *B*). The basic argument is that the former reversible behavior is suggestive of dissociation at the receptor-ligand binding site (adhesive detachment mode), whereas the latter irreversible behavior is indicative of disruption at the protein-membrane anchor site (cohesive detachment mode). It was found that the detachment modes were correlated with the types of molecular bonds involved (e.g., receptor-ligand binding versus antibody-antigen binding) (Chesla et al., 1995). A quantitative measure of the extraction probability, or irreversibility, can be derived from the statistical analysis of the binding evolution curves (Chesla et al., 1997) (Chesla et al., manuscript in preparation).

The receptor (CD16A) and ligands (IgG) employed in this work were found to form weak bonds that would most likely dissociate at detachment. In fact, analyses of all of the binding evolution curves that gave rise to all of the adhesion probability data shown in Fig. 10 demonstrated small probabilities of uprooting compared to the extraction probability in the case in which the bonds were mediated by Leu-11b-CD16A binding (cf. Fig. 4 *B*). While this low extraction probability is not required for the insurance of the rate constants determined by the present method to be those governing the binding of receptors and ligands rather than their membrane anchoring, it does justify the use of the running frequency at the last test as the best estimate for the adhesion probability. For declining running frequency, the measurement of adhesion probability requires fitting of the entire binding evolution curve to a Markov process model, as exemplified in Fig. 4 *B* (Chesla et al., manuscript in preparation). Unlike reversible binding, where the adhesion probability is independent of the test cycle count, the adhesion probability for the irreversible binding decreases with the test cycle count. Nevertheless, its extrapolated initial value before the first test can be used for the purpose of employing the present method. Using such initial P_a data, the theoretical analysis described herein can still be applied to evaluate the kinetic rates for receptor-ligand binding, despite the fact that measurement of this binding probability results in uprooting of receptors and/or ligands in such a case (Chesla et al., 1997, and manuscript in preparation).

Further support for the Poisson approximation

The method described in this paper includes a systematic approach to determining the kinetic mechanism. The 1:1 stoichiometry of the 2D adhesion determined by the present work is in agreement with that measured in 3D binding (Ghirlando et al., 1995). The analyses presented in the Results have clearly demonstrated the feasibility and illustrated the strategy of the approach. The analysis was greatly enhanced by the closed-form solution, Eq. 5, which forms the basis of several novel graphical representations of the

data (Figs. 8–10). From Fig. 2, the condition for the Poisson type of approximate solution (Eq. 5 if $\nu_b = 1$) to be valid is $A_c m_{min} \gg (\nu_r/\nu_b)\langle n\rangle$, which, when all stoichiometric coefficients are unity, becomes $K_a^0 m_{max} \ll 1$ (cf. Eq. 5b). From the values listed in Table 1, it can be seen that this condition is satisfied for all m_{max} values tested, justifying the use of the Poisson approximation. When P_a is plotted against the average number of bonds, $\langle n\rangle$ (Fig. 12), all of the P_a versus t data shown in Fig. 10 collapse into a single curve, regardless of the individual values of k_f^0, k_r^0, m_r, m_l, and t, further supporting the Poisson approximation and demonstrating the same kinetic mechanism for the two IgG ligands from different origins.

Comparison to the deterministic kinetic model

In addition to the master equations, Eq. 2, its deterministic counterpart, the large system limit of Eq. 3a (with $\sigma_n^{(\nu_r+\nu_l)} = \sigma_n^{(\nu_b)} = 0$), or rather, that of the Poisson approximate master equations (the $\nu_b = 1$ case),

$$\frac{d}{dt}\left(\frac{\langle n\rangle}{A_c}\right) = k_f^0 m_r^{\nu_r} m_l^{\nu_l} - k_r^0\left(\frac{\langle n\rangle}{A_c}\right), \tag{11}$$

was tested for the ability of its solution ($\langle n\rangle/A_c$) to fit the measured P_a versus t data. It is interesting to note that Eq. 11 is identical to Eq. A15, and hence predicts exactly the same solution for $\langle n\rangle$ as that given by Eq. 5b. Given the nearly linear relationship between P_a and $\langle n\rangle$ when they are small (see Fig. 12), it is not surprising that Eq. 11 was also able to fit the data, yielding comparable rate constants (not shown).

However, we cannot emphasize enough that major conceptual differences exist between the deterministic and probabilistic viewpoints. In large systems appropriate for the deterministic description, the fraction of molecules in the bound state is small initially; and only when the contact time approaches the reciprocal per cell forward rate constant, $1/(A_c m_r m_l k_f^0)$, will the number of bonds become comparable to that of the total reacting molecules. Because the number of receptors and ligands participating in binding is enormous, however, even a very small fraction of these represent many molecules. Therefore, bond formation must occur as soon as the two cell membranes are placed in contact. Similarly, dissociation takes place immediately after bonds are formed, despite the fact that the fraction of bonds dissociated is small until the contact time is comparable to the reciprocal reverse rate constant, $1/k_r^0$. In the transient phase of the $\langle n\rangle/A_c$ versus t curve, bond formation outpaces bond dissociation, whereas the two processes reach an equal rate in the plateau phase.

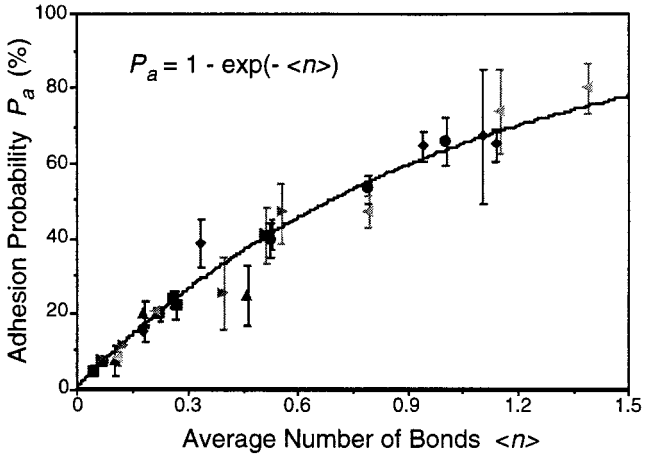

FIGURE 12 The probability of specific adhesion, P_a, was plotted against the average bond number, $\langle n\rangle$, which was calculated based on Eq. 5b, using the two pairs of evaluated kinetic rate constants (Table 1, the two "combined data" rows for human and rabbit IgG, respectively). All data (*points*) collapsed into a single curve, which is in excellent agreement with the indicated theoretical solution (*curve*). The error bars were computed from the original data by using the Gaussian error propagation law.

In small systems, by comparison, only a few or even no bond may form during the entire contact time, for one no longer has large numbers of molecules interacting simultaneously. As illustrated in Fig. 13 *A*, bond formation may occur at any instant during the contact time, or it may not occur at all. Moreover, bonds formed at an earlier instant after the beginning of contact may dissociate at a later instant before the end of the contact. In any particular adhesion test, when an adhesion is detected during cell-cell separation, the experimenter does not know the precise moment in the contact period when the bonds are formed. Similarly, when no adhesion is detected, he does not know whether this is a case in which the bonds formed at earlier instants have already dissociated, or it is the case in which there is no bond formation at all. Nevertheless, one thing is certain and measurable in repeated adhesion tests: the probability of adhesion and its changes with the contact time. Thus, from the probabilistic standpoint, it is the likelihood of bond formation (as opposed to bond formation itself) that outpaces the likelihood of bond dissociation (as opposed to bond dissociation itself) in the transient phase of the P_a versus t curve. In the plateau phase the changes in the two likelihoods reach an equal rate.

It should be noted that, in small systems appropriate for the probabilistic description, the time scales set forth by $1/(A_c m_r m_l k_f^0)$ and $1/k_r^0$ reflect the respective waiting times necessary for the events of bond formation and dissociation to occur, not the actual durations of these events. The physical processes during which the binding pockets of the receptor and ligand fit into or break away from one another take place on a much much shorter time scale ($\sim \mu$s or even ns; Bell, 1978), as illustrated in Fig. 13 *A* by instantaneous jumps. The waiting time is limited by diffusion (predominantly the rotational and orientational modes rather than the translational mode).

Effect of finite time requirement for adhesion detection

The beginning of the contact period is operationally defined as the instant when the piezo-driven micropipette first ar-

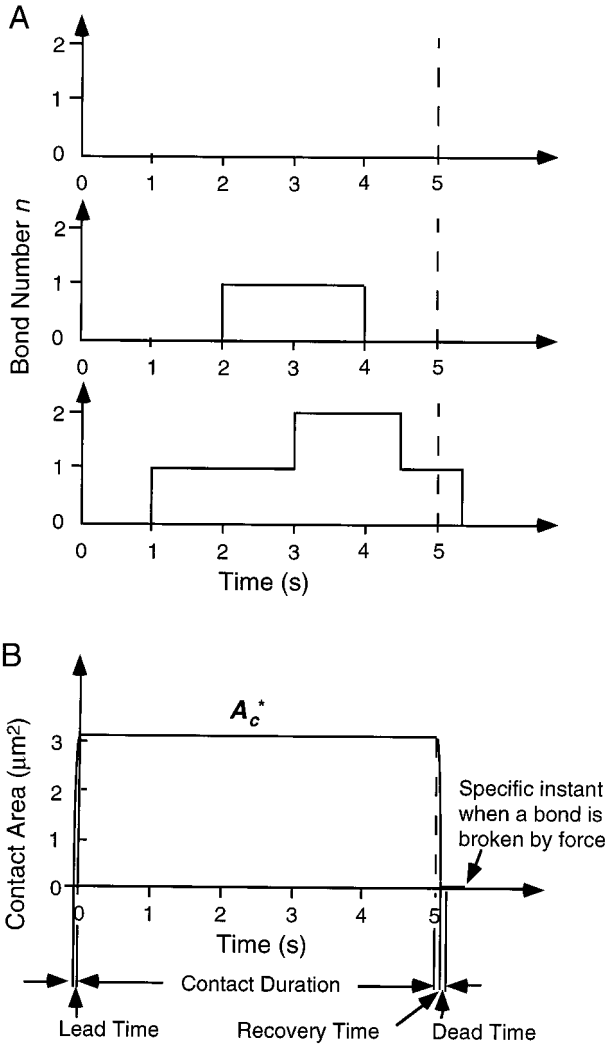

FIGURE 13 (*A*) Three example realizations of the bond number, *n*, as a stochastic process in time, *t*, during the cell-cell contact. The changes in *n* appear as random jumps of unit step size that could take place at any instant. Either formation of a new bond (*n* is increased by 1) or dissociation of a preformed bond (*n* is decreased by 1) may occur. (*Top*) No bond formation occurred during the entire 5 s of contact duration. (*Middle*) A bond was formed at 2 s but dissociated at 4 s. In both cases, no adhesion was detected by the experimenter, and he would not be able to tell the different between the two. (*Bottom*) Two bonds were formed at the 1- and 3-s time points respectively. Adhesion was detected in the postcontact cell-cell separation phase at the end of the dead time (5.1-s time point), after which the bond was broken by force at the 5.3-s time point. However, the experimenter would not know that more than one bond was formed, but one dissociated at the 4.5-s time point before the end of the contact duration. (*B*) Schematic of how the apparent contact area changes with time, indicating the definitions of lead time, contact duration, recovery time, and dead time. Note that the apparent contact area A_c^* ($= \pi D^2/4$, where $D \approx 2$ μm is the apparent contact diameter measured from photomicrographs such as that shown in Fig. 1 *A*) is proportional, but not necessarily equal to the true contact area A_c. Also indicated is the instant at which the bond shown in the bottom panel of *A* was broken by force.

rives at its pause position and stops motion (Fig. 13 *B*). At this moment, the contact area has achieved a plateau level; this is defined as A_c. To arrive at this finite contact area, however, requires a nonvanishing time (called *lead time*) that precedes the above-defined beginning instant of the contact period and which starts when the two cell membranes first come into point contact (Fig. 13 *B*).

Similarly, the end of the contact period is operationally defined as the instant when the experimenter starts to pull the cells apart, but at this moment the cells are still in touch with one another (Fig. 13 *B*). In a process that is the reversal of what occurred in the lead time, the RBC membrane gradually reassumes its uncompressed shape upon the removal of the impingement force (assuming that adhesion, if any, occurs at the apex); the time of this process is called the *recovery time* (Fig. 13 *B*).

Theoretical treatment of the variable contact area during the lead time and the recovery time is possible by replacing the constant A_c in Eq. 2 with a (given) function of time; but this will greatly increase the mathematical complexity of the analysis. Such a treatment seems not to be warranted, for the overall effect of not including in the analysis the lead time and recovery time must be minimal. Adhesions that occurred in the lead time would be included as adhesions that occurred during contact time. In contrast, bond formation and dissociation that occurred in the recovery time would not be included, as they could not be detected by the experimenter. Thus the individual effects of excluding the lead time and recovery time from analysis cancel one another.

The experimenter cannot tell whether adhesion has occurred until the RBC has been further withdrawn, resulting in either a deflection in its membrane (Fig. 1 *C* or *D*) or a separation of its spherical outline from the CHO cell (Fig. 1 *B*). This is also a process that takes nonvanishing time (called *dead time*) to accomplish. Formation of new adhesions during dead time is highly unlikely because of the vanishing contact area. However, bonds preformed during the contact time but dissociated in the dead time (probably at a faster rate because of the influence of force) cannot be counted. The effect of such a dead time is analyzed below.

Because $0.5/k_r^0$ is the contact time needed for the adhesion probability to reach half-maximum (cf. Eq. 10c), some of the P_a data ought to be measured in contact times shorter than $0.5/k_r^0$ for both kinetic rate constants (as opposed to just the binding affinity) to be resolved, as measurements at longer contact times where the adhesion probability levels off contain only equilibrium information. In the present work, $0.5/k_r^0 \approx 1.4$ and 2.5 s for CD16A binding to human and rabbit IgG, respectively. Two contact time points (0.5 and 1 s) shorter than $0.5/k_r^0$ were used. In our experiments, the piezoelectric translator withdrew the micropipette at a speed of 10 μm/s. A 0.5-μm withdrawal, which is quite enough for the experimenter to determine whether adhesion has occurred, required only 0.05 s. Such a dead time is an order of magnitude shorter than the shortest contact duration and 30–50 times shorter than $0.5/k_r^0$. This ensures that the adhesion events that occurred during the dead time would be negligible compared to those that occurred during the contact time, validating the applicability of the present method to the CD16A-IgG system.

However, if the receptor-ligand interaction in question dissociates with a fast rate such that its $0.5/k_r^0$ is comparable to the dead time, then bond dissociation becomes likely to occur in the dead time. This would result in an underestimation of the adhesion frequency if contact times comparable to $0.5/k_r^0$ were used. To minimize such an effect, much longer contact times must be used to ensure that binding events that take place in the contact time would remain dominant over those that occur in the dead time. Consequently, only steady-state, not transient data can be reliably measured, yielding only the binding affinity, not kinetic rate constants.

Thus it is of interest to reduce the dead time as much as possible. However, withdrawing the RBC too fast would induce significant hydrodynamic forces that deform the cell. Moreover, rapid deflections of the RBC would be resisted by the membrane viscosity in addition to elasticity. Both effects would reduce the sensitivity of the RBC force transducer. Using the Stokes equation, $F = 6\pi\eta R_c V$, the drag force F a spherical RBC (of radius $R_c = 2.5\ \mu$m) experiences as it moves in a medium of viscosity $\eta = 10^{-3}$ pN · s/μm^2 at a speed of $V = 10\ \mu$m/s can be found to be 0.5 pN, much smaller than the typical single bond strength. However, using a Voigt model for the RBC membrane with a membrane viscosity $\eta_m \approx 0.6$–1.2 pN · s/μm (Hochmuth, 1987), the viscous resistance to a 10 μm/s deformation rate would be 6–12 pN, on the same order of magnitude as the typical single bond strength. Indeed, we found that a pipette retraction speed much greater than 10 μm/s resulted in notable reduction of the frequency of detectable adhesions.

Effect of low force detection limits

The value of the forward rate constant predicted by the present method depends on several factors. One of these is whether the adhesion probability estimate takes all positive adhesion scores into account. This requires that even a single receptor-ligand bond be unambiguously detected. To achieve this ultrahigh level of sensitivity, the human red blood cell was used as the adhesion detector (Fig. 1). The micropipette aspirated RBC force transducer has been shown to be capable of detecting forces as low as subpiconewtons, which is orders of magnitude lower than the typical strength of a noncovalent receptor-ligand bond (Bell, 1978; Evans et al., 1991; Chesla and Zhu, 1996; Zhu and Chesla, 1997). However, dissociation of such noncovalent receptor-ligand bonds is a stochastic event that could occur at any force, even at zero force (Bell, 1978; Evans et al., 1991; Zhu and Chesla, 1997). As such, there would always be a fraction of positive adhesions that are inevitably miscounted as false negative nonadhesions. The impact of this detection limit is examined below.

Let α_n be the fraction that is miscounted in those adhesion events that are mediated by n bonds, because of the sensitivity cutoff of the adhesion detector. The relationships $\alpha_n \geq 0$ and $\alpha_n > \alpha_{n+1}$ ($n \geq 1$) must hold, as the more bonds that are involved in the adhesion, the harder it is for it to dissociate at low force, and hence the smaller the miscounted fraction. For simplicity, the α_n's are assumed to be parameterized as $\alpha_n = \alpha^n$ ($0 \leq \alpha < 1$). This equation is probably not exact, but it should be a reasonable approximation. The advantage of using such a power law expression with a single parameter is that it enables a close-form solution. Discounting these fractions from the "ideal" adhesion probability, $P_{ai} = 1 - p_0$, the "actual" adhesion probability, P_{aa}, detected by the experimenter, the one that ought to be used to fit the data, should be

$$P_{aa} = P_{ai} - \sum_{n=1}^{\infty} \alpha^n p_n = 1 - \sum_{n=0}^{\infty} \frac{(\alpha\langle n\rangle)^n}{n!} \exp(-\langle n\rangle)$$
$$= 1 - \exp\{-(1-\alpha)A_c m_r m_l K_a^0[1 - \exp(-k_r^0 t)]\}. \quad (12)$$

It follows from Eq. 12 that, as a result of detection cutoff, the binding affinity (and thereby the forward rate constant) would be underestimated by a factor of $1 - \alpha$, whereas the reverse rate constant is not affected (compared to the equation in Fig. 6).

Effects of receptor and ligand availability

Other factors affecting the value of k_f^0 (and K_a^0) derived from the present work have to do with the availability of the receptors and ligands in the contact area. In contrast to k_r^0, which has the same unit (s^{-1}) on both the per-cell and per-molecular density basis, the per molecular density k_f^0 (in μm^2 s^{-1}) was not computed directly from the fitting of the P_a versus t data. Instead, it was lumped into a per-cell forward binding rate constant, $A_c m_r m_l k_f^0$ (s^{-1}). To calculate k_f^0 from $A_c m_r m_l k_f^0$ requires separate experiments to independently measure the densities of receptors, m_r, and ligands, m_l, as well as the contact area, A_c.

Two assays were employed in the present study to measure m_r and m_l: flow cytometry and radioimmunoassay. As can be seen in Fig. 3, either assay allowed for consistent quantification of CD16A expressed on CHO cells and IgG coated on RBCs. However, whereas soluble antibodies used in these assays could access all surface antigens, it is likely that ligands coating the RBCs were only able to access those receptors that were localized on the tips of the microvilli, but not those that were hidden in the membrane folds of the rough surface of a CHO cell. It is not known whether the CD16A molecules are evenly distributed on the CHO cell surface, as are β_2 integrins on neutrophils, or are concentrated on the microvilli tips, as are L-selectin and PSGL-1 on neutrophils (Hasslen et al., 1996). Should it be the former case, the number of molecules capable of participating in binding ought to be its density (molecule per cell/total area per cell) times the area of the microvillus tips in the contact, not the apparent contact area. Taking an estimated 100% excess membrane over a spherical cell of radius 10 μm and assuming the microvilli to be cylinders 0.5 μm long and 0.1

μm in diameter, it can be estimated that only 2.5% of the apparent contact area measured from the photomicrograph ($\sim$3 μm^2 in all experiments; cf. Fig. 1 *A*) can be counted as true A_c.

Although the surface of a RBC is much smoother than that of a CHO cell, not all of the ligands necessarily have a proper orientation that is recognizable by the cell-bound receptors, as the chromium chloride method employed to coat the RBC surface with IgG is not specific. We have investigated this issue, and the details will be described elsewhere (Chesla et al., manuscript in preparation). Briefly, it was found that, of the ligands capable of interacting with soluble antibodies in the surface density determination (the values listed in Table 1 for m_l), only a small fraction ($\sim$10–20%) are functioning in cell adhesion. The kinetic parameters reported in Table 1 were calculated assuming all IgG molecules detected by flow cytometry in site density determination were functioning; thus the values for k_f^0 (and K_a^0) are underestimated.

In addition, the total human IgG used in this study includes all four subtypes, of which only two, hIgG1 and hIgG3, bind to CD16 (Nagarjan et al., 1995). Because they comprise $\sim$70% (hIgG1) and 5% (hIgG3), respectively, of the total hIgG, the kinetic rate constants calculated here are average properties of CD16A binding to the two subtypes of hIgG. Experiments are under way to measure the intrinsic kinetic properties of each subtypes of hIgG1 and hIgG3.

Despite the uncertainty associated with dissecting the per molecular density forward rate constant k_f^0, the values of the per-cell forward rate constant, $A_c m_r m_l k_f^0$, and the reverse rate constant, k_r^0, should be unambiguous and directly relevant to predicting cellular behavior, as they were evaluated directly from the cell adhesion data. It is interesting to note that these two parameters are of the same order of magnitude as those measured for E-selectin/carbohydrate ligand binding by the flow chamber method (Kaplanski et al., 1993). Because the kinetic rates are believed to determine whether the receptor-ligand interaction is rapid enough to capture moving cells in the flow environment, we tested whether Fcγ receptors could mediate adhesion of flowing cells to a hIgG-coated surface. Preliminary results suggest that this is indeed the case (Wright, 1997).

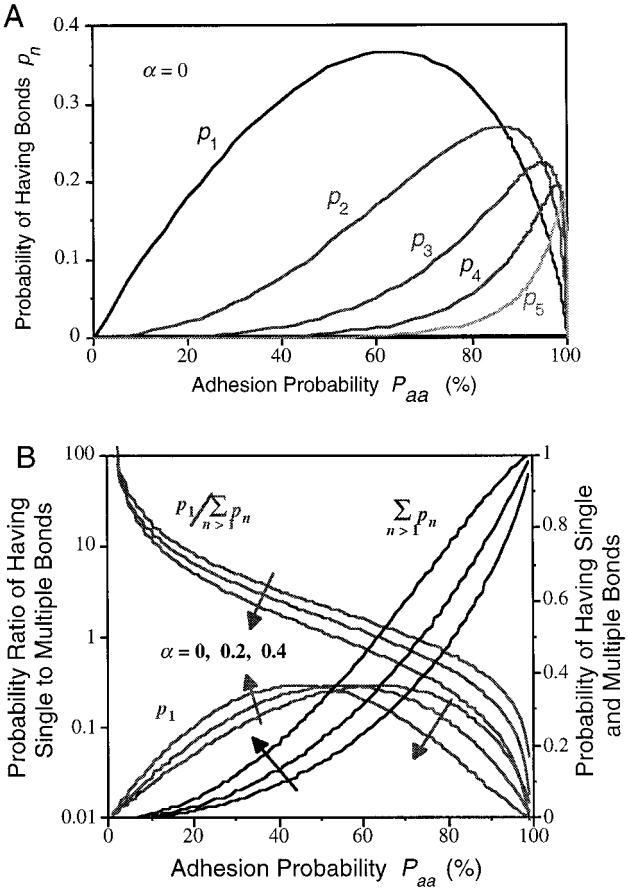

FIGURE 14 Individual bond feature of the present method. (*A*) Probabilities of having the first five bonds, p_n (n = 1–5), and (*B*) that of having single, p_1, and multiple, $\Sigma_{n>1}p_n$, bonds (*right ordinate*), as well as the ratio of the probability of having a single bond to that of having multiple bonds, $p_1/\Sigma_{n>1}p_n$, (*left ordinate*) as a function of the measured probability of adhesion per contact, P_{aa}, and the fraction of miscounting false nonadhesions, α.

Individual molecular features of the method

An interesting observation from Fig. 12 is the smallness of the average number of bonds ($\langle n \rangle < 1.5$) that mediate the adhesion seen in our experiments. To further explore this low bond number feature, the P_{aa} versus $\langle n \rangle$ relationship (Eq. 12) was used to eliminate $\langle n \rangle$ from Eq. 5 to obtain a prediction for the bond distribution as a function of adhesion probability:

$$p_n = \frac{(1 - P_{aa})^{1/(1-\alpha)}}{n!} \ln^n (1 - P_{aa})^{-1/(1-\alpha)}. \qquad (13)$$

It can be seen from Fig. 14 *A* that, even with the highest adhesion probability seen in our experiments, the number of bonds that have nonvanishing probabilities ($\geq$0.01) is no more than five. If $\alpha = 0$, $p_1 > p_n$ for $n > 1$, even at P_{aa} = 80%. For moderate and low adhesion probabilities, the bindings are mediated predominantly by single bond events, although this dominance is weakened somewhat as α increases (Fig. 14 *B*).

The above low bond number prediction is also consistent with the observation in the micropipette experiment that, although the two cells were allowed to touch each other via an apparent area of a few square microns during the contact period, only very few (usually only one if at all) spatially separate discrete attachment point(s) were observed when the contact was being separated (Fig. 1, *C* and *D*). One might argue that it was still possible that multiple bonds were involved in these point attachments. For this to be the case, however, the receptors and ligands must either be multivalent or be presented on their respective cell surfaces as clusters, such that bonding of one binding site in the multivalent molecule (or one molecule in the cluster) dramatically increases the probability that the other binding

sites in the same multivalent molecule (or other molecules in the same cluster) will bind, leading to the rapid formation of multiple bonds as a single unit in a discrete attachment point of vanishing area, despite the fact that the odds of forming more new bonds in the rest of the contact area of much larger size remains low. The CD16A-IgG binding is monovalent, as shown in the Results and by Ghirlando et al. (1995). Furthermore, it is unlikely that both CD16A and IgG are clustered on their respective cell membranes. Thus, not only does our micropipette method measure the adhesion kinetics of individual cells; it also is very likely to probe the binding kinetics of individual molecules. It should be emphasized that the method does not require all adhesions to be single bond mediated, as the analysis utilizes not only single but also multiple bond events. In other words, the small fraction of multiple bond events contributes useful information, not noise, to the analysis.

CONCLUSION

A novel method has been developed for measuring the kinetic rate constants in cell adhesion. The method is based on a combined experimental assay and a mathematical model. The assay is designed to measure the adhesion probability. Although the protocol was illustrated by the micropipette technique in this work, it should be adaptable to other techniques, such as the atomic force microscope (Hinterdorfer et al., 1996). Several analytical solutions to the master equations were presented. Systematic strategies have been developed to determine the kinetic mechanism and the associated rate constants of the binding reaction. The model has been supported by careful experimental validation of the underlying assumptions and satisfactory agreements between data and predictions.

APPENDIX: SOLUTION TO THE MASTER EQUATIONS

The binomial distribution

Under the condition of the first simplified case, Eq. 2 (with $\nu_r = \nu_l = \nu_b = 1$) can be approximated by a set of master equations that correspond to a kinetic mechanism of first-order reversible reaction between the free and bound states of the limiting species:

$$\frac{dp_n}{dt} = [A_c m_{min} - (n-1)]m_{max}k_f^0 p_{n-1} - [(A_c m_{min} - n)m_{max}k_f^0 + nk_r^0]p_n + (n+1)k_r^0 p_{n+1}. \quad \text{(A1)}$$

Following McQuarrie (1963), Eq. A1 can be solved using the approach of a probability-generating function, defined by

$$g(x,t) = \sum_{n=0}^{\infty} x^n p_n(t). \quad \text{(A2)}$$

Upon partially differentiating Eq. A2 with respect to time and substituting Eq. A1 into the right-hand side of the resulting equation, the original system of $A_c m_{min} + 1$ coupled first-order linear ordinary differential equations in p_n is converted into a single first-order linear partial differential equation in g:

$$\frac{\partial g}{\partial t} + [m_{max}k_f^0 x^2 + (k_r^0 - m_{max}k_f^0)x - k_r^0]\frac{\partial g}{\partial x} = A_c m_r m_l k_f^0 (x-1)g. \quad \text{(A3)}$$

Two particular solutions to Eq. A3 were discussed by McQuarrie (1963), which satisfy, respectively, the initial condition that there are $A_c m_{min}$ bonds initially or that the initial bonds are distributed binomially. We have found the general solution by using the method of characteristics (Zauderer, 1983),

$$g = J\{(x-1)\exp(-kt)/[x + (m_{max}K_a^0)^{-1}]\}[x + (m_{max}K_a^0)^{-1}]^{A_c m_{min}}, \quad \text{(A4)}$$

where J is an arbitrary integration function of its argument, $u = (x-1)\exp(-kt)/[x + (m_{max}K_a^0)^{-1}]$, to be determined by the initial conditions. The parameters have been defined in the main text.

Without losing generality, let us consider the case in which there are m ($0 \le m \le A_c m_{min}$) bonds initially, as the solution to the general case of an arbitrary initial condition can easily be obtained from the solutions of these special cases by using the principle of superposition. The initial conditions for the probabilities, namely,

$$p_{n|m} = \delta_{nm} = \begin{cases} 1 & n = m \\ 0 & n \ne m \end{cases} \quad \text{at } t = 0, \quad \text{(A5)}$$

can be translated into an initial condition for the probability-generating function g_m, i.e.,

$$\left.\frac{\partial^m g_m}{\partial x^m}\right|_{t=0} = m! \quad \text{and} \quad \left.\frac{\partial^k g_m}{\partial x^k}\right|_{\substack{t=0\\x=0}} = 0 \quad \text{for} \quad 0 \le k < m, \quad \text{(A6a,b)}$$

where the subscript m indicates the condition of m initial bonds. For fixed value of t (= 0), Eq. A6a is an mth order of ordinary differential equation, whereas Eq. A6b is the initial conditions. Integration of these yields

$$g_m(x,0) = x^m. \quad \text{(A7)}$$

Setting $t = 0$ in Eq. A4 and comparing it with Eq. A7, the functional form of J_m can now be determined:

$$J_m(u) = [1 + (m_{max}K_a^0)^{-1}]^{-A_c m_{min}}[1 + (m_{max}K_a^0)^{-1}u]^m \cdot (1-u)^{A_c m_{min} - m}. \quad \text{(A8)}$$

With the substitution of Eq. A8 into Eq. A4, the probability generating function g_m is determined:

$$g_m(x,t) = \left\{\frac{x + (m_{max}K_a^0)^{-1}[1 + (x-1)e^{-kt}]}{1 + (m_{max}K_a^0)^{-1}}\right\}^m \cdot \left[\frac{x + (m_{max}K_a^0)^{-1} - (x-1)e^{-kt}}{1 + (m_{max}K_a^0)^{-1}}\right]^{A_c m_{min} - m}. \quad \text{(A9)}$$

For the particular case in which there is no bond initially, setting $m =$

0 in Eq. A9 and expanding the resulting equation into Taylor series in terms of x yields

$$g_0(x,t) = \sum_{n=0}^{A_c m_{min}} x^n \binom{A_c m_{min}}{n} \left[\frac{1-\exp(-kt)}{1+(m_{max}K_a^0)^{-1}}\right]^n \cdot \left[1-\frac{1-\exp(-kt)}{1+(m_{max}K_a^0)^{-1}}\right]^{A_c m_{min}-n}. \quad \text{(A10)}$$

Comparing to Eq. A2, the coefficient of x^n in the sum in Eq. A10 can readily be identified as the binomial distribution given by Eq. 4.

The Poisson distribution

Under the condition of the second simplified case, Eq. 2 (with $\nu_b = 1$) is reduced to

$$\frac{dp_n}{dt} = A_c m_r^{\nu_r} m_l^{\nu_l} k_f^0 p_{n-1} - (A_c m_r^{\nu_r} m_l^{\nu_l} k_f^0 + n k_r^0) p_n + (n+1) k_r^0 p_{n+1}. \quad \text{(A11)}$$

We have found exact solutions to Eq. A11 by using a probability-generating function approach similar to that employed in the preceding section (see Long et al., manuscript submitted for publication). An alternative approach is presented below, which can also be used to obtain the binomial solution (Piper, 1997).

The solution is assumed to be of the form of the Poisson distribution. This is reasonable because, under the above simplifying assumptions, making a contact between the two surfaces is equivalent to simultaneously conducting an infinitely large number of independent identical tests, each consisting of an attempt by a molecule to bind the countermolecule, with a vanishingly small probability of forming a bond. The product of the test number and the probability, however, is finite and equal to the average number of bonds formed, $\langle n\rangle$. Thus the probability of having n bonds is given by Eq. 5a. Equation 5a was differentiated with respect to time and rearranged to give two possible forms,

$$\frac{dp_n}{dt} = (p_{n-1} - p_n)\frac{d\langle n\rangle}{dt}$$

and (A12a,b)

$$\frac{dp_n}{dt} = [np_n - (n+1)p_{n+1}]\frac{1}{\langle n\rangle}\frac{d\langle n\rangle}{dt}.$$

Multiplying Eq. A12a by λ and Eq. A12b by $1-\lambda$, and then adding the two resulting equations yields

$$\frac{dp_n}{dt} = \{\lambda p_{n-1} - [\lambda + n(\lambda-1)/\langle n\rangle]p_n + [(n+1)(\lambda-1)/\langle n\rangle]p_{n+1}\}\frac{d\langle n\rangle}{dt}. \quad \text{(A13)}$$

Comparing Eqs. A13 and A11 to identify like terms yields

$$\lambda\frac{d\langle n\rangle}{dt} = A_c m_r^{\nu_r} m_l^{\nu_l} k_f^0 \quad \text{and} \quad \frac{\lambda-1}{\langle n\rangle}\frac{d\langle n\rangle}{dt} = k_r^0. \quad \text{(A14a,b)}$$

Eliminating λ from Eqs. A14a and A14b results in a simple equation for $\langle n\rangle$:

$$\frac{d\langle n\rangle}{dt} + k_r^0\langle n\rangle = A_c m_r^{\nu_r} m_l^{\nu_l} k_f^0, \quad \text{(A15)}$$

the solution of which is

$$\langle n\rangle = \langle n\rangle_0 \exp(-k_r^0 t) + A_c m_r^{\nu_r} m_l^{\nu_l} K_a^0[1-\exp(-k_r^0 t)], \quad \text{(A16)}$$

where integration constant $\langle n\rangle_0$ is the average bond number at $t = 0$, which is zero under the initial condition given by Eq. 1. Equation A16 thus becomes Eq. 5b.

It can be seen from the above derivation that only those solutions to Eq. A11 whose initial conditions satisfy Poisson distribution can be obtained by this alternative approach. By comparison, the probability-generating function approach is able to handle any initial conditions.

We thank Ping Li for the CHO cells expressing CD16A and SCD16A. This work was supported by National Science Foundation grants BCS 9210684 and 9350370, National Institutes of Health grant AI38282 (CZ), and NIH grant AI30631 (PS). SEC was also partially supported by NIH training grant GM08433.

REFERENCES

Alon, R., S. Chen, K. D. Puri, E. B. Finger, and T. A. Springer. 1997. The kinetics of L-selectin tethers and the mechanics of selectin-mediated rolling. *J. Cell Biol.* 138:1169–1180.

Alon, R., D. A. Hammer, and T. A. Springer. 1995. Lifetime of the P-selectin-carbohydrate bond and its response to tensile force in hydrodynamic flow. *Nature.* 374:539–542.

Bell, G. I. 1978. Models for the specific adhesion of cells to cells. *Science.* 200:618–627.

Berenson, R. J., W. I. Bensinger, and D. Kalamasz. 1986. Positive selection of viable cell populations using avidin-biotin immunoadsortion. *J. Immunol. Methods.* 91:11–19.

Boyce, W. E., and R. C. DiPrima. 1977. Elementary Differential Equations and Boundary Value Problem, 3rd Ed. John Wiley and Sons, New York.

Capo, C., F. Garrouste, A.-M. Benoliel, P. Bongrand, A. Ryter, and G. Bell. 1982. Concanavalin-A-mediated thymocyte agglutination: a model for a quantitative study of cell adhesion. *J. Cell Sci.* 56:21–48.

Chen, S., R. Alon, R. C. Fuhlbrigge, and T. A. Springer. 1997. Rolling and transient tethering of leukocytes on antibodies reveal specializations of selectins. *Proc. Natl. Acad. Sci. USA.* 94:3172–3177.

Chesla, S. E., B. T. Marshall, and C. Zhu. 1997. Measuring the probability of receptor extraction from the cell membrane. *In* 1997 Advances in Bioengineering, BED-Vol. 36. B. Simon, editor. ASME, New York. 129–130.

Chesla, S. E., P. Selvaraj, and C. Zhu. 1995. The mechanics of single molecular interactions between Fc gamma receptor III (CD16) isoforms and their ligands. *In* Proceedings of the 1995 Bioengineering Conference, BED-Vol. 29. R. M. Hochmuth, N. A. Langrana, and M. S. Hefzy, editors. ASME, New York. 455–456.

Chesla, S. E., and C. Zhu. 1996. Validation and accuracy assessment of the micropipet piconewton force transducer. *In* 1996 Advances in Bioengineering, BED-Vol. 30. S. Rastegar, editor. ASME, New York. 77–78.

Cozens-Roberts, C., D. A. Lauffenburger, and J. A. Quinn. 1990. Receptor-mediated cell attachment and detachment kinetics. I. Probabilistic model and analysis. *Biophys. J.* 58:841–856.

Delobel, J. 1992. Quantification of the adhesion force between individual promyelocytic cells and Kaposi's sarcoma cells using a micropipette technique. M.S. thesis. Georgia Institute of Technology, Atlanta.

Dustin, M. L., L. M. Ferguson, P.-Y. Chan, T. A. Springer, and D. E. Golan. 1996. Visualization of CD2 interaction with LFA-3 and determination of the two-dimensional dissociation constant for adhesion receptors in a contact area. *J. Cell Biol.* 132:465–474.

Evans, E., D. Berk, and A. Leung. 1991. Detachment of agglutinin-bonded red blood cells. I. Forces to rupture molecular-point attachments. *Biophys. J.* 59:838–848.

Evans, E. A., and K. Ritchie. 1994. Probing molecular attachments to cell surface receptors: image of stochastic bonding and rupture processes. *In* Scanning Probe Microscopies and Molecular Materials. J. Rabe, H. E. Gaub, and P. K. Hansma, editors. Kluwer Publishing, Amsterdam.

Evans, E. A., K. Ritchie, and R. Merkel. 1995. Sensitive force technique to probe molecular adhesion and structural linkages at biological interfaces. *Biophys. J.* 68:2580–2587.

Ghirlando, R., M. B. Keown, G. A. Mackay, M. S. Lewis, J. C. Unkeless, and H. J. Gould. 1995. Stoichiometry and thermodynamics of the interaction between the Fc fragment of human IgG1 and its low-affinity receptor FcγRIV. *Biochem.* 34:13320–13327.

Gold, E. R., and H. H. Fudenberg. 1967. Chromic chloride: a coupling reagent for passive hemoagglutination reactions. *J. Immunol.* 99: 859–866.

Hasslen, S. R., A. R. Burns, S. I. Simon, C. W. Smith, K. Starr, A. N. Barclay, S. A. Michie, R. D. Nelson, and S. L. Erlandsen. 1996. Preservation of spatial organization and antigenicity of leukocyte surface molecules by aldehyde fixation: flow cytometry and high-resolution FESEM studies of CD62L, CD11b, and Thy-1. *J. Histochem. Cytochem.* 44:1115–1122.

Hinterdorfer, P., W. Baumgartner, H. Gruber, K. Schilcher, and H. Schindler. 1996. Detection and localization of individual antibody-antigen recognition events by atomic force microscopy. *Proc. Natl. Acad. Sci. USA.* 93:3477–3481.

Hochmuth, R. M. 1987. Properties of red blood cells. *In* Handbook of Bioengineering. R. Skalak and S. Chien, editors. McGraw-Hill, New York.

Hulett, M. D., and P. M. Hogarth. 1994. Molecular basis of Fc receptor function. *Adv. Immunol.* 57:1–127.

Kaplanski, G., C. Farnarier, O. Tissot, A. Pierres, A. Benoliel, M. C. Alessi, S. Kaplanski, and P. Bongrand. 1993. Granulocyte-endothelium initial adhesion: analysis of transient binding events mediated by E-selectin in a laminar shear flow. *Biophys. J.* 64:1922–1933.

Kofler, R., and G. Wick. 1977. Some methodologic aspects of the chromium chloride method for coupling antigen to erythrocytes. *J. Immunol. Methods.* 16:201–209.

Kwong, D., D. F. J. Tees, and H. L. Goldsmith. 1996. Kinetics and locus of failure of receptor-ligand-mediated adhesion between latex spheres. II. Protein-protein bond. *Biophys. J.* 71:1115–1122.

Lawrence, M. B., and T. A. Springer. 1991. Leukocytes roll on a selectin at physiological flow rates: distinction from and prerequisite for adhesion through integrins. *Cell.* 65:859–873.

Leckband, D. E., F. J. Schmitt, J. N. Israelachvili, and W. Knoll. 1994. Direct force measurements of specific and nonspecific protein interactions. *Biochemistry.* 33:4611–4624.

McQuarrie, D. A. 1963. Kinetics of small systems. I. *J. Chem. Phys.* 38:433–436.

Nagarjan, S., S. E. Chesla, L. Cobern, P. Anderson, C. Zhu, and P. Selvaraj. 1995. Ligand binding and phagocytosis by CD16 (FcγRIII) isoforms: phagocytic signaling by associated ζ and γ subunits in CHO cells. *J. Biol. Chem.* 270:25762–25770.

Pierres, A., A.-M. Benoliel, and P. Bongrand. 1995. Measuring the lifetimes of the bonds made between surface-linked molecules. *J. Biol. Chem.* 270:26586–26592.

Pierres, A., A.-M. Benoliel, and P. Bongrand. 1996a. Experimental study of the rate of bond formation between individual receptor-coated spheres and ligand-bearing surfaces. *J. Phys. III France.* 6:807–824.

Pierres, A., A.-M. Benoliel, and P. Bongrand. 1996b. Measuring bonds between surface-associated molecules. *J. Immunol. Methods.* 196: 105–120.

Piper, J. W. 1997. Force dependence of cell bound E-selectin/carbohydrate ligand binding characteristics. Ph.D. thesis. Georgia Institute of Technology, Atlanta.

Piper, J. W., R. A. Swerlick, and C. Zhu. 1998. Determining force dependence of two-dimensional receptor-ligand binding affinity by centrifugation. *Biophys. J.* 74:492–513.

Press, W. H., B. P. Flannery, S. A. Teukolsky, and W. T. Vetterling. 1989. Numerical Recipes in FORTRAN: The Art of Scientific Computing. Cambridge University Press, Cambridge, England.

Scatchard, G. 1949. The attraction of proteins for small molecules and ions. *Ann. N.Y. Acad. Sci.* 51:660–672.

Selvaraj, P., W. F. Rosse, R. Silber, and T. A. Springer. 1988. The major Fc receptor in blood has a phosphatidylinositol anchor and is deficient in paroxysmal nocturnal hemoglobinuria. *Nature.* 333:565–567.

Setiadi, H., S. L. Erlandsen, and R. P. McEver. 1998. Interactions of the cytoplasmic domain of P-selectin with clathrin-coated pits enhance neutrophil adhesion under flow. *J. Cell Biol.* (in press).

Sung, K.-L. P., L. A. Sung, M. Crimmins, S. J. Burakoff, and S. Chien. 1986. Determination of junction avidity of cytolytic T cell and target cell. *Science.* 234:1405–1408.

Tees, D. F. J., O. Coenen, and H. L. Goldsmith. 1993. Interaction forces between red cells agglutinated by antibody. IV. Time and force dependence of break-up. *Biophys. J.* 65:1318–1334.

Tees, D. F. J., and H. L. Goldsmith. 1996. Kinetics and locus of failure of receptor-ligand-mediated adhesion between latex spheres. I. Protein-carbohydrate bond. *Biophys. J.* 71:1102–1114.

Unanue, E. R. 1984. Antigen-presenting function of the macrophage. *Annu. Rev. Immunol.* 2:395–428.

van de Winkel, J. G., and P. J. Capel. 1993. Human IgG Fc receptor heterogeneity: molecular aspects and clinical implications. *Immunol. Today.* 14:215–221.

von Andrian, U. H., J. D. Chambers, L. M. McEvoy, R. F. Bargatze, K. E. Arfors, and E. C. Butcher. 1991. Two-step model of leukocyte-endothelial cell interactions in inflammation: distinct roles for LECAM-1 and the leukocyte β_2-integrins in vivo. *Proc. Natl. Acad. Sci. USA.* 88:7538–7542.

Wright, D. A. 1997. The adherence of tumor cells to endothelial cells and of neutrophils to IgG, under flow. M.S. thesis. Georgia Institute of Technology, Atlanta.

Zhu, C., and S. E. Chesla. 1997. Dissociation of individual molecular bonds under force. *In* 1997 Advances in Bioengineering, BED-Vol. 36. B. Simon, editor. ASME, New York. 177–178.

Zhu, C., J. W. Piper, and R. A. Swerlick. 1998. A centrifugation method for measurement of two-dimensional binding characteristics of receptor-ligand interaction. *In* Bioadhesion in Drug Delivery: Issues in Fundamentals, Novel Approaches, and Development. E. Mathiowitz, C. M. Lehr, and D. Chickering, editors. Marcel Dekker, New York.